

Mott Experiment Run I/II Data Analysis

Daniel Moser

JLAB-TN-17-025

June 2017

Abstract

This note describes the analysis code used to analyze individual Mott data runs and analysis performed outside of the code. Choices of cuts in the analysis code and accounting of systematic and statistical sources of uncertainty is discussed along with exploration of background and dilution. Finally, asymmetries and rates from Runs I and II for a given foil thickness are presented.

Table of Contents

1. Analysis Code

• Summary	3
• First Loop	3
• Second Loop – Calculating Asymmetries	11
• Second Loop – Calculating Rates	14
• Scaler Loop	16

2. Choice of Cuts

• Time-of-Flight Cuts	18
• Energy Cuts	23
• Sensitivity to Choice of Cuts	25
◦ Asymmetry Grid	26
◦ Average Rate Grid	28
◦ Effect on Final Fits	31

3. Background Within Our Cuts

4. Final Asymmetry Calculation

5. Final Rate Calculation

6. Run I Summary of Results

7. Run II Summary of Results

8. Asymmetry Without Time-of-Flight Cut 43

Analysis Code – Summary

The Mott DAQ produces a raw data file for each data run that is then decoded into a ROOT tree such that each scaler has a unique branch. The analysis consists of ROOT-interpretted C++ code that an individual run's ROOT tree is passed to.

There are three main sub-routines in the Mott analysis code that are executed sequentially – the first loop in which time-of-flight and energy spectra are fit in order to determine “good” elastic scatterings from the target foil; the second loop in which the determined “good” scatterings are broken down by helicity and asymmetries are calculated along with rates; and the scaler loop in which charge asymmetry is calculated.

Analysis Code – First Loop

From a run's ROOT tree, in the first loop sub-routine, “raw” data histograms are filled. Eight histograms corresponding to each of the 8 PMTs – Left, Right, Up, Down for Energy and dEnergy – are filled. These histograms are helicity-independent, that is, events with either helicity state are present.

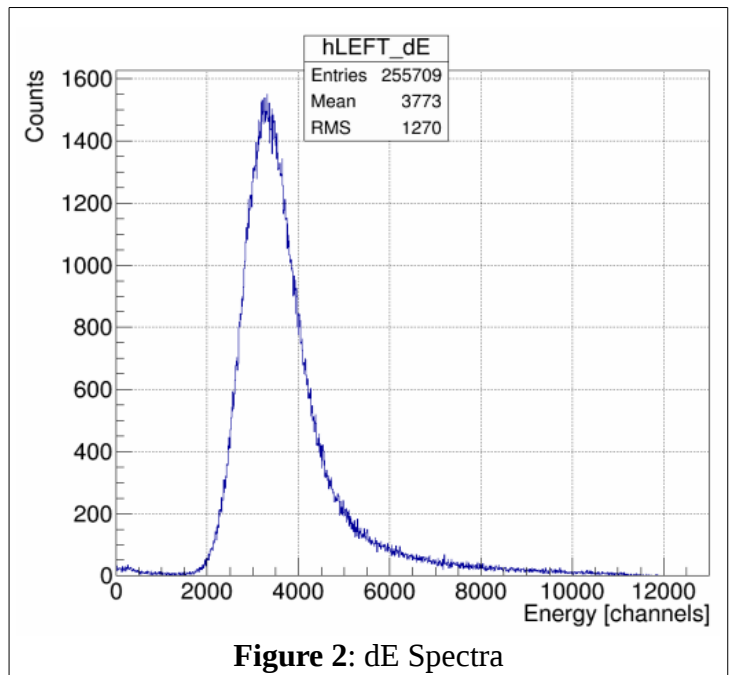
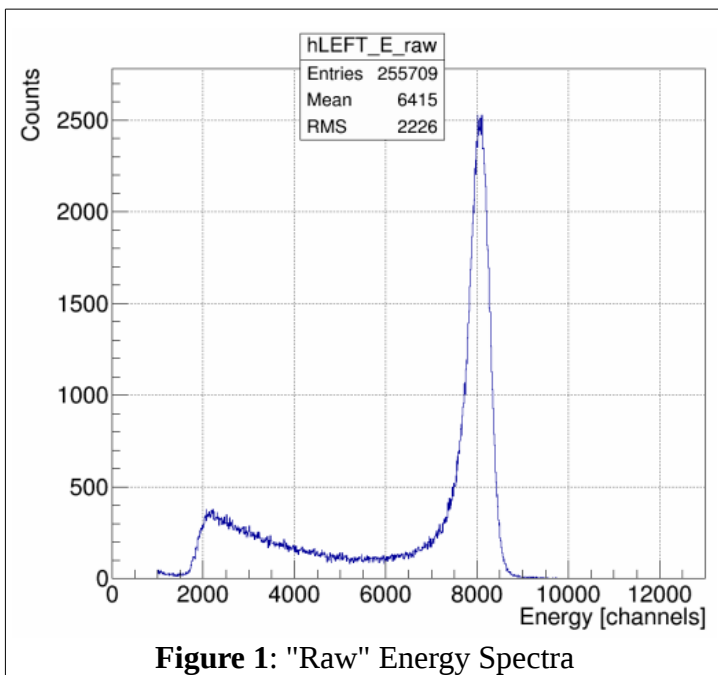
The energy for each of the events in these histograms is calculated by recording 50 sample raw detector signals from the DAQ's FADC. Then, taking the average of the first 10 of these samples, an average pedestal p is calculated. This pedestal is then subtracted from each of the next 40 samples, which are summed together, producing the event's energy in units of channels.

$$p = \frac{1}{10} \sum_{i=0}^9 FADC_i \quad (1)$$

$$E[\text{channels}] = \sum_{i=10}^{49} (FADC_i - p) \quad (2)$$

PMT histograms are binned 10Ch/Bin from 0 to 13000. Time-of-flight (ToF) histograms for each detector are also filled at this time. These histograms are binned 10 bins/ns, or 100 ps/bin (TDC resolution is 34ps/channel), from 40 to 80 ns. Additionally, for display, 2-dimensional Energy vs ToF, dE vs ToF, and Energy vs dE histograms are created. The energy axis follows the same binning as the 1D histograms, while ToF axis is expanded to a 90 ns window and 2 bins/ns. The full width of a coincidence window is 100 ns.

Figures 1 through 6 are sample spectra from the Left detector of Mott Run 8545 – Run II, 31MHz beam repetition rate, vertically linearly polarized electrons, scattering off of a 350 nm gold foil. Corresponding spectra for the other three detectors are similar. Figure 1 shows a typical E-detector “raw”, or uncut, spectra. The elastic target scatterings peak occurs around channel 8000. The channel this peak occurs at corresponds to the beam's kinetic energy, which for run 8545 = 4.917 ± 0.013 MeV. Figure 2 shows a typical dE-detector spectra. Figures 3 shows a typical Time-of-Flight spectra with a log-scale y-axis. Run 8545 was performed with a hardware timing veto wired into the FADC, and so from roughly 61 to 74 ns there appears to be no data. Without this veto, a second peak corresponding to scatterings from the dump would be present, and in Figure 1, the energy spectra background signal – channel < 6000 – would be greater. The peak around 54 ns is scatterings from the target foil. Figure 4 shows “raw” energy spectra vs ToF, Figure 5 dE vs ToF, and Figure 6 E vs dE.



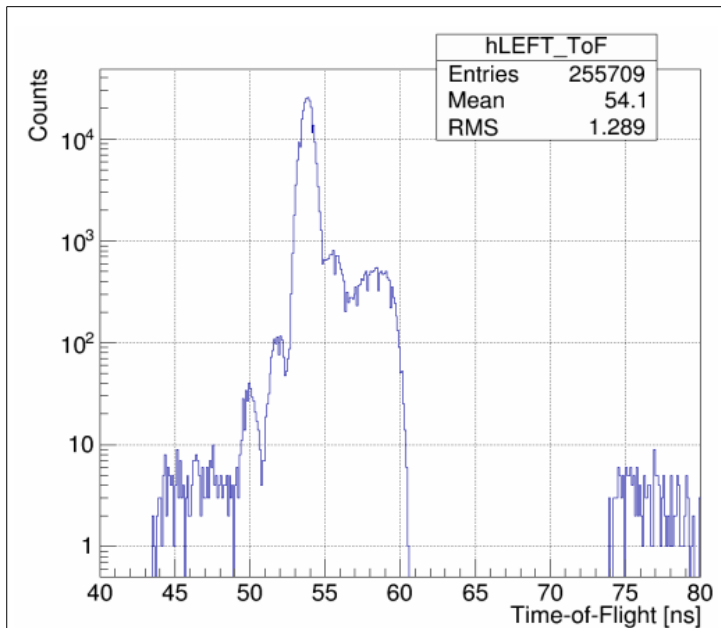


Figure 3: Time-of-Flight Spectra, Vertical Log Scale

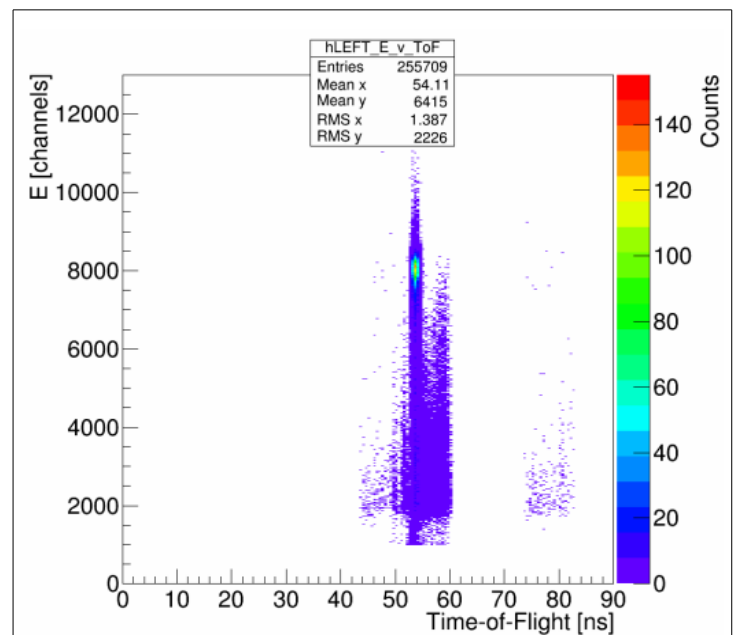


Figure 4: Energy vs Time-of-Flight

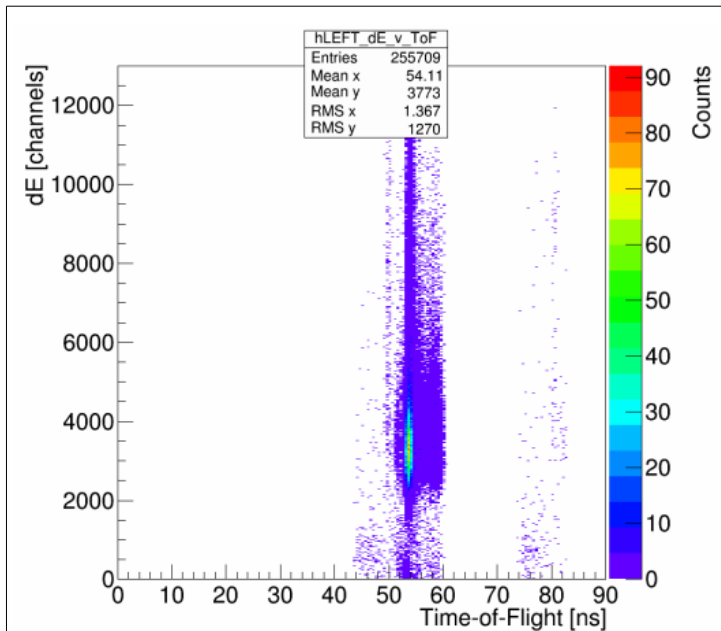


Figure 5: dE vs Time-of-Flight

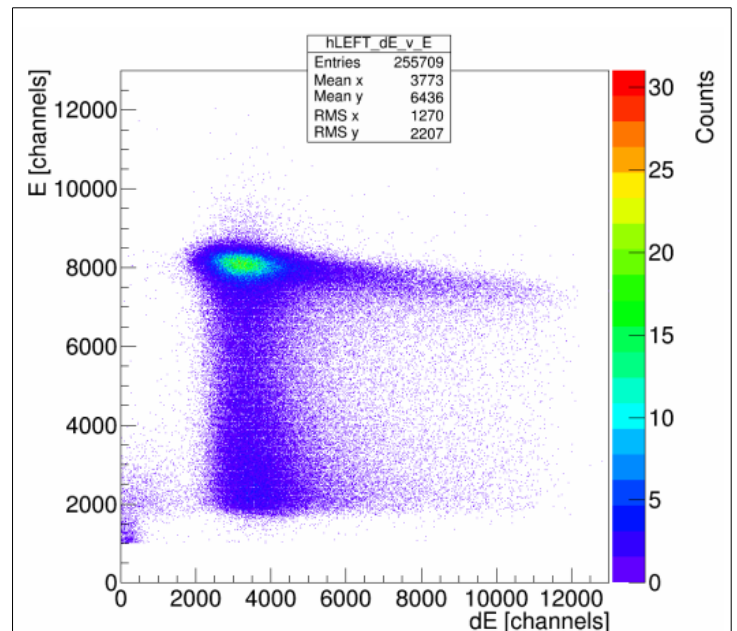
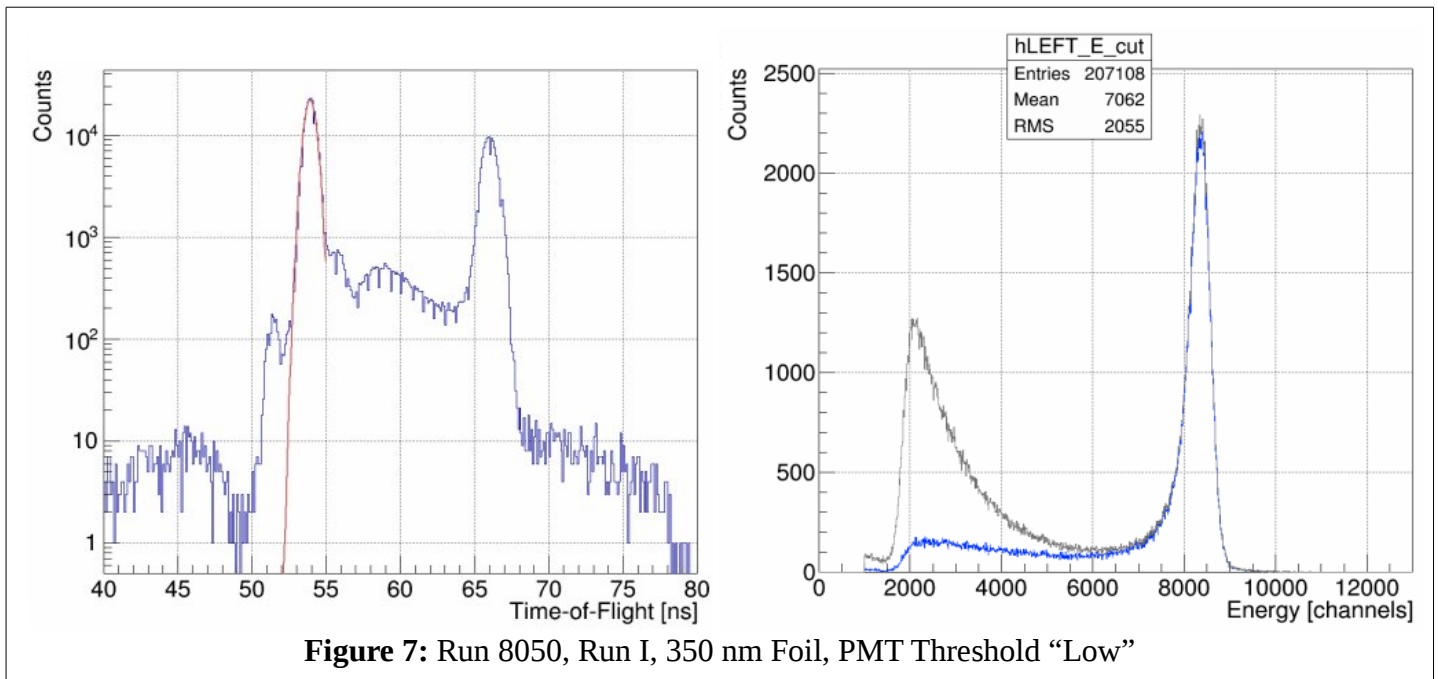
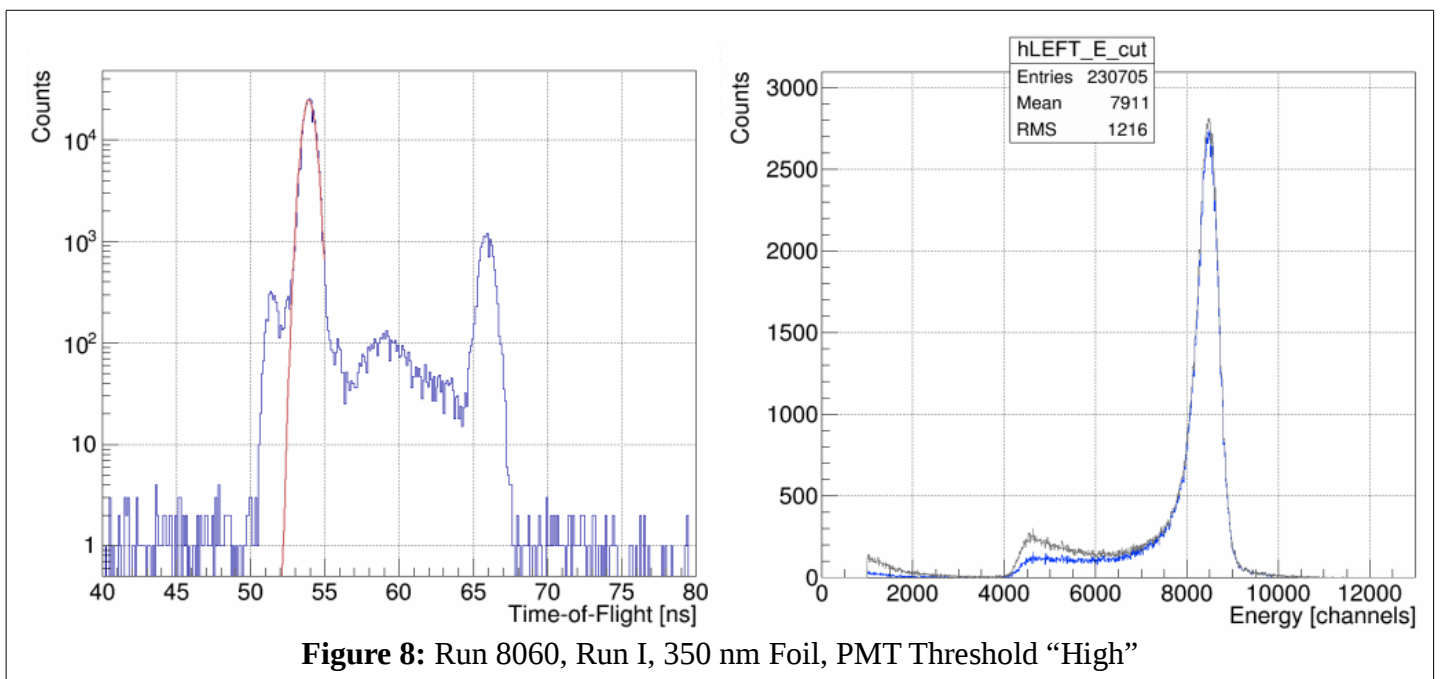


Figure 6: Energy vs dE

For comparison, Figures 7 and 8 show runs 8050 and 8060's Left detector ToF and Energy spectra. Both of these runs are from Run I on identical 350 nm gold foils, 31 MHz beam repetition rate, and with no hardware timing veto installed. Unlike in run 8545, there are two distinct peaks in the ToF-spectra of these runs – first at 54 ns corresponding to target scatterings, and second at 66 ns corresponding to scatterings off of the dump. The gray trace in the energy spectra plot in Figure 7, an uncut energy spectra from a run *without* a timing veto can be compared with Figure 1, a run on the



same foil but from Run II *with* a timing veto. Without a timing veto the background (Channel < 6000) is much greater. Apart from the two copies of the 350 nm foils, the only difference between 8050 and 8060 is they were performed with different PMT high-voltage settings – 8050 with “low” HV threshold, 8060 with “high” HV threshold. This affects the the energy spectra by shifting the lowest-energy event resolved to higher and higher energies, and so further to the right, as HV on the PMTs is raised. For “low” PMT threshold, run 8050, the leftmost channel is ~2250, for “high” PMT threshold, run 8060, the leftmost channel is ~4500.



After filling histograms, when running at a suitable beam repetition rate, each detector's ToF spectra's target peak is fit with a Gaussian – red curve on the ToF spectra in Figures 7 and 8. To do this, the maximum bin between 49 and 55 ns is found and used as the seed value for the mean of the Gaussian fit. The amplitude seed value is 1000 counts, and the sigma seed value is 1 ns, both chosen heuristically. The fit is restricted to the 49 to 55 ns range. The default ROOT TH1 class fitter is used – a χ^2 function minimized using Minuit and the MIGRAD minimizer. From this fit, the time-window that “good” Mott scattering events from the target foil occur within is determined as from (mean – 2 sigma) to (mean + 2 sigma). The choice of this ± 2 sigma window about the mean is explained in detail in section **Choice of Cuts – Time-of-Flight**. Then, the uncut, “raw” energy spectra are Time-of-Flight cut – for each Left, Right, Up, Down detector, a new energy histogram is filled, but only if the event occurs within our specified time-window. Figures 7 and 8 show uncut energy spectra in gray and corresponding ToF-cut spectra in blue.

When making Mott measurements with beam repetition rates of 249.5 MHz or 499 MHz, typical CEBAF repetition rates, the beam bunches are temporally spaced too close together to resolve a target scattering peak in the Time-of-Flight spectra. In this case, a flag can be passed to the analysis code to forgo the fit and subsequent ToF cut.

Next in the first-loop subroutine, ToF-cut energy spectra (or simply “raw” energy spectra if no ToF-cuts are possible or wanted) are horizontally normalized such that their peaks each line up at a specified energy channel “center,” chosen to be 8000. This is implemented by calculating a 'squeeze fraction' equal to the center of the bin that the maximum count value occurs at divided by the channel to center on. Then, any bin edge or bin center can be calculated simply as:

$$\text{NewBin} = (\text{MaxCountBinCenter} / \text{center}) * \text{OldBin} \quad (3)$$

thereby squeezing/centering our four different detector energy spectra about a chosen channel. Figure 9 shows unnormalized horizontally ToF-cut energy spectra from run 8545 in gray, and horizontally normalized ToF-cut energy spectra in blue. Figure 10 then shows the horizontally normalized, ToF-cut energy spectra of each of the four detectors atop one another. Because both helicity-states are present in each of the four detectors, an asymmetry in Left/Right or Up/Down detector pairs is not apparent.

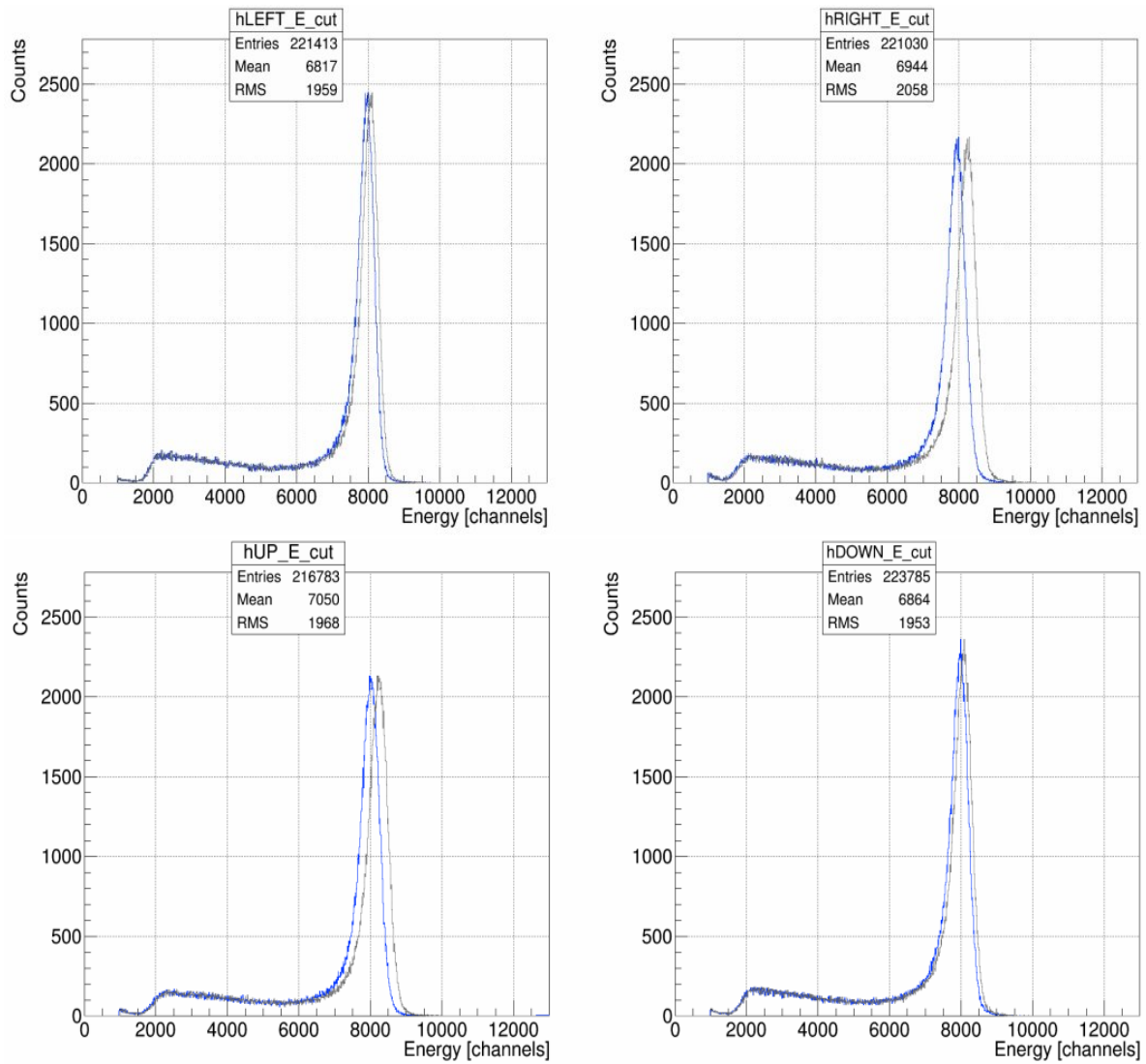


Figure 9: Horizontally Normalizing, from gray to blue, ToF-Cut Energy Spectra

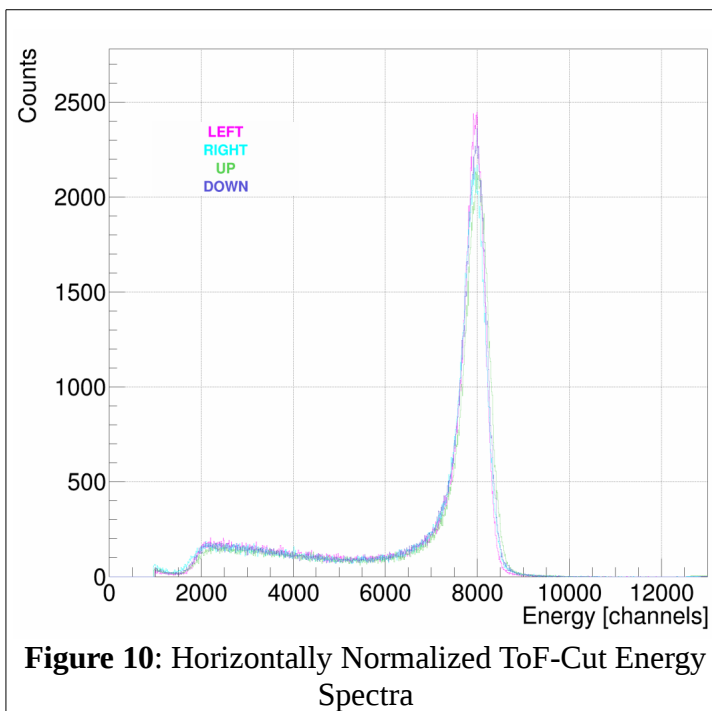
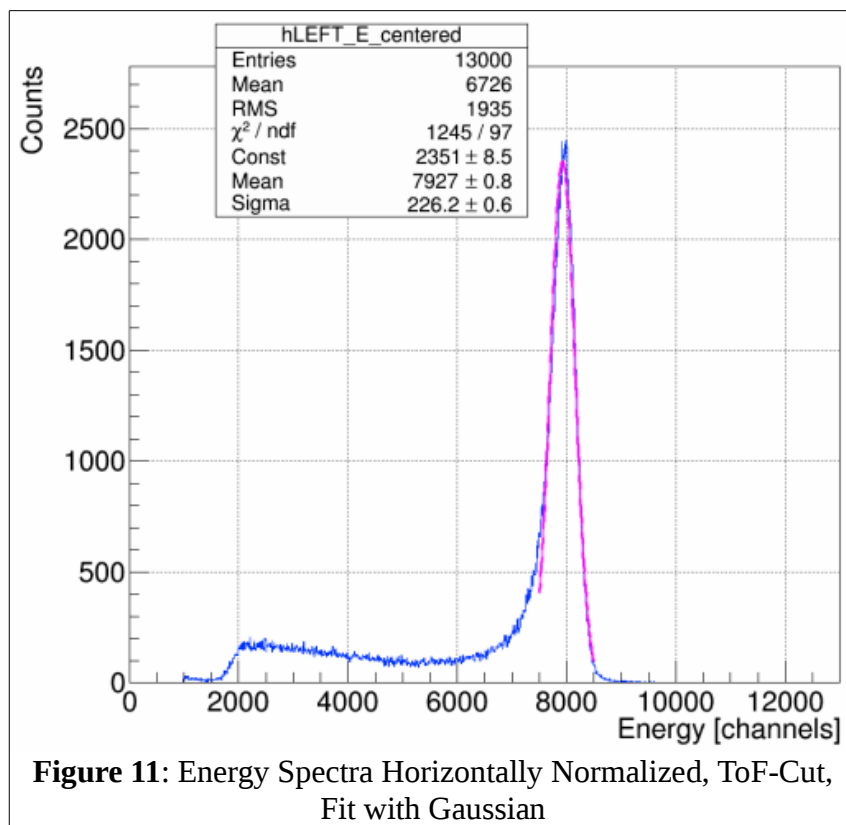


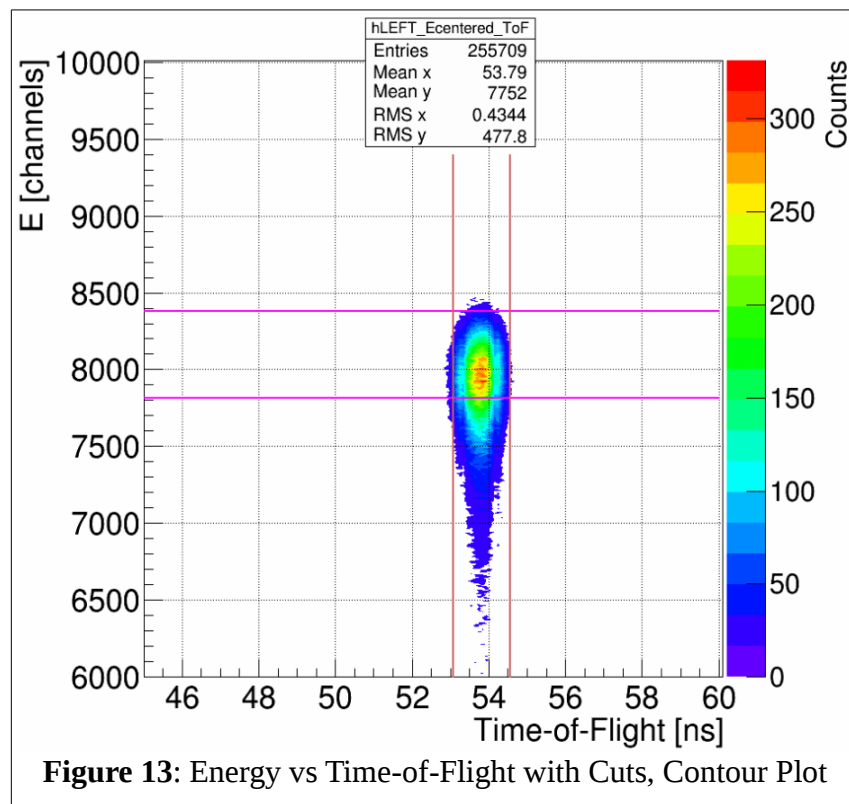
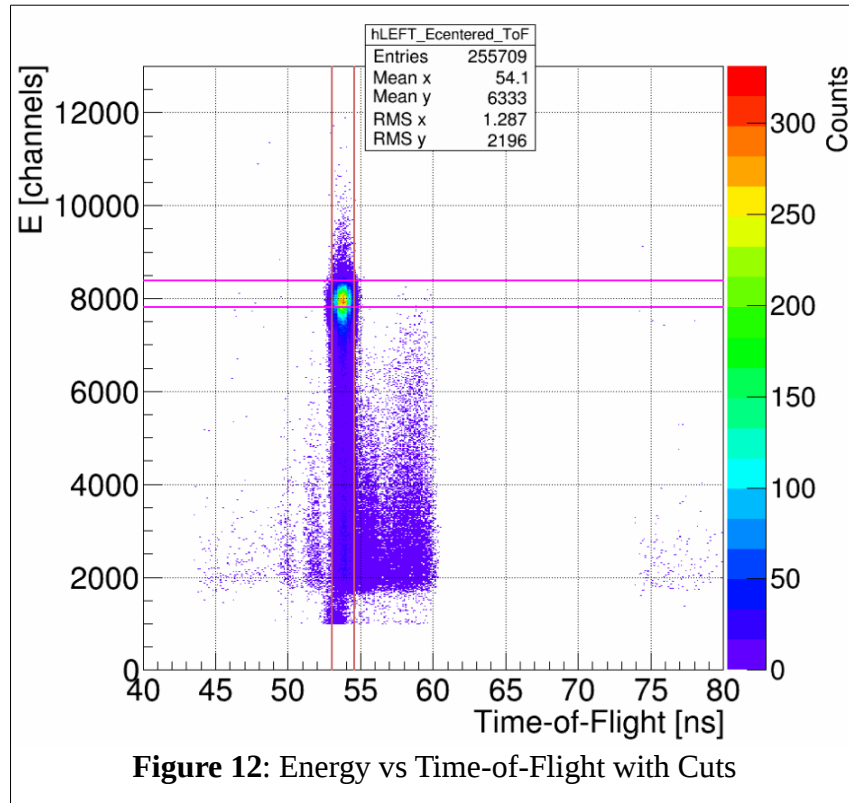
Figure 10: Horizontally Normalized ToF-Cut Energy Spectra



Next, each of the four detectors' horizontally normalized, potentially ToF-cut, energy spectra is fit with a Gaussian. The mean is given the “center” bin used to horizontally normalize about as its seed value, meanwhile the amplitude and sigma are each given a seed value heuristically determined to be 300. The fit is restricted to +/-500 channels about the “center” bin. Again, the default ROOT TH1 fitter is used. Figure 11 shows run 8545's Left detector energy spectra, ToF-cut, horizontally normalized about channel 8000, fit with a Gaussian in magenta. From the returned fit parameters, a “good” elastic scatterings off the target foil energy window is determined as from $(\text{mean} - (\frac{1}{2})\text{sigma})$ to $(\text{mean} + 2\text{sigma})$. The choice of this energy-cut window is explained in detail in section **Energy Cuts**.

Just prior to the end of the first loop subroutine, fit parameters and associated uncertainties from both fits along with 'squeeze fractions' are written to a formatted output file. The Time-of-Flight and Energy windows determined by the fits, windows that define our “good” Mott scatterings off the target foil, are passed to the second loop along with the calculated 'squeeze fractions' to horizontally normalize energy spectra. Figures 12 and 13 show run 8545's Left detector Energy vs Time-of-Flight plot with the determined Time-of-Flight window/cut shown by the vertical light red lines and the Energy window/cut shown by the horizontal magenta lines. Figure 13 is a contour rather than scatter

plot. These figures differ from Figure 4 in that the energy data is horizontally normalized about the chosen center bin. They are also generated in the second loop rather than the first, although it could be done in either.



Analysis Code – Second Loop, Calculating Asymmetries

In the second loop subroutine, from a given run's ROOT tree, eight new energy spectra histograms are filled – four E-detectors, and now breaking down scatterings by positive or negative helicity state. These histograms are binned exactly like previous E and dE-detector histograms – 0 to 13000 channels, 10 Channels/bin. Only scatterings that make it within our energy window determined in the first loop, within our time-of-flight window if one is employed, and that have a well-defined helicity, are added. Using the 'squeeze fractions' passed from the first loop, these “good” elastic scatterings from the target foil are added directly to their horizontally normalized bin.

Continuing the use of run 8545 from Run II, we have vertically linearly polarized incident electron beam scattering off a 350nm gold foil, and so we expect to observe physics asymmetry in the Left and Right E-detectors. Figure 14 shows these E-detectors, broken down by helicity.

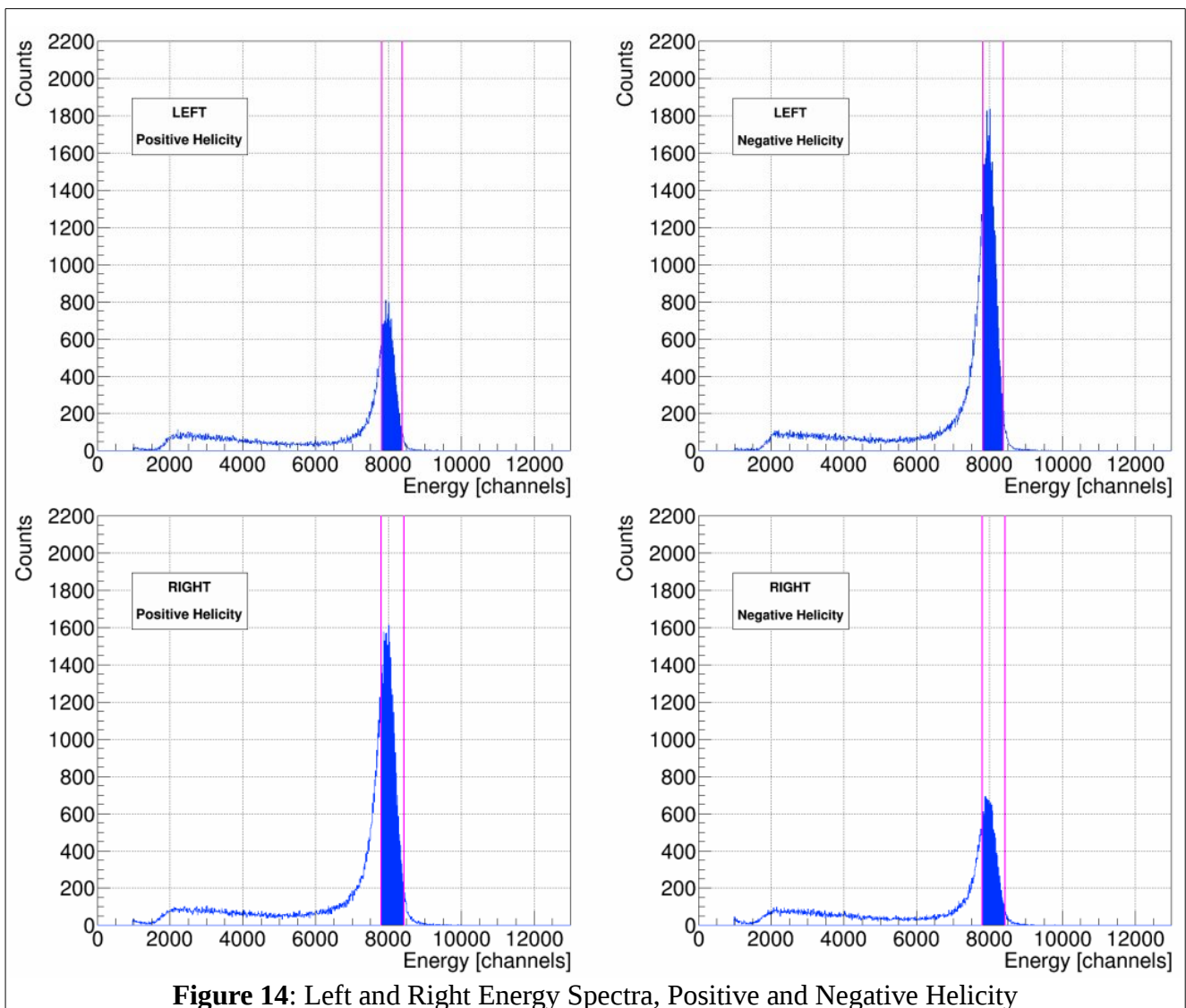
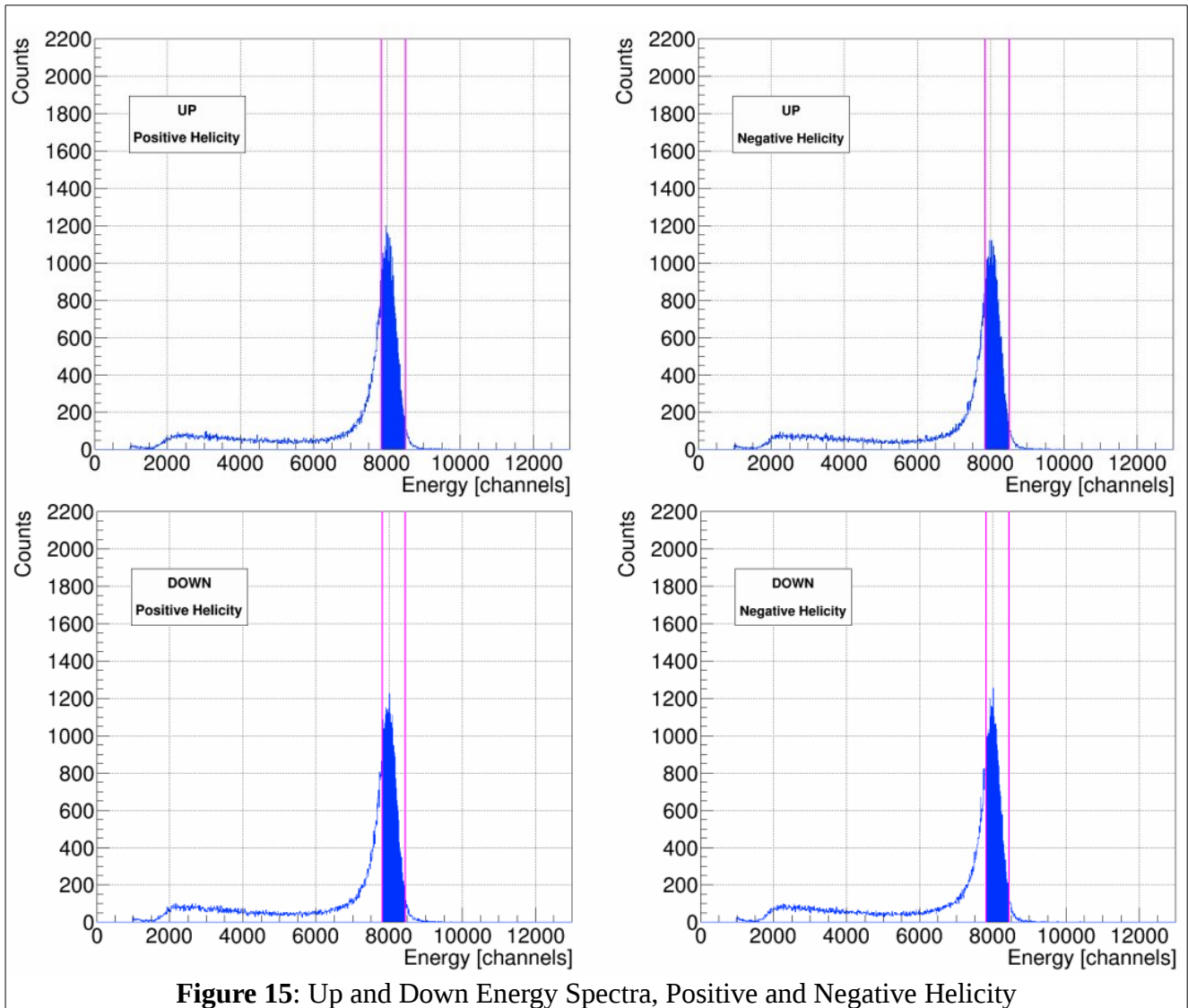


Figure 14: Left and Right Energy Spectra, Positive and Negative Helicity

The difference in height between positive and negative helicity in one detector, as well as between Left and Right detectors for a given helicity, indicate non-zero asymmetry. These spectra are horizontally normalized and Time-of-Flight cut. Magenta lines are used to show our energy-cut window. Filled in blue represent the “good” elastic scatterings we will use in our asymmetry calculations, the scatterings that fall within both our Time-of-Flight and Energy cuts. For contrast, Figure 15 shows the Up/Down E-Detectors helicity spectra from Run 8545– all four are approximately the same height, indicating little to no asymmetry in this plane.



With our “good” elastic Mott scatterings determined, we can now calculate asymmetries using the cross-ratio method. The cross-ratio method is advantageous for our purposes in that the physics asymmetry is independent – cancels to all orders – of relative detector efficiencies and solid angles, of

relative integrated charge, and of target thickness variation. The differences in beam polarization in the two helicity states, however, only cancels to first order. Reference [1], G. G. Ohlsen, Jr. and P. W. Keaton, Nuclear Instruments Methods 109 (1973), “Techniques for Measurement of Spin-½ and Spin-1 Polarization Tensors,” discusses in detail the advantages and limitations of the cross-ratio method, and the effects of misalignments, false asymmetries, and spin-angle uncertainty. Derivations of asymmetry calculations used in the analysis, Equation 4 the physics or Mott asymmetry measured A , Equation 6 the detector instrumental asymmetry $Instr_1$, and Equation 8 the beam instrumental asymmetry $Instr_2$, are also presented.

Let L^+ = number of positive helicity “good” elastic Mott scatterings counted in the Left E-detector, L^- = number of negative helicity “good” elastic Mott scatterings counted in the Left E-detector, and so forth for $R^{+/-}$, $U^{+/-}$, and $D^{+/-}$. Then, considering only the Left-Right plane for the moment, the cross-ratio method gives us for physics/Mott asymmetry A –

$$r = \sqrt{\frac{L^+ R^-}{L^- R^+}}$$

$$N = \sqrt{\frac{1}{L^+} + \frac{1}{L^-} + \frac{1}{R^+} + \frac{1}{R^-}}$$

$$A = \frac{1 - r}{1 + r} \quad (4)$$

$$dA = \frac{N \cdot r}{(1 + r)^2} \quad (5)$$

For detector instrumental asymmetry $Instr_1$ (note the different definition or “ r ”) –

$$r = \sqrt{\frac{L^+ L^-}{R^+ R^-}}$$

$$N = \sqrt{\frac{1}{L^+} + \frac{1}{L^-} + \frac{1}{R^+} + \frac{1}{R^-}}$$

$$Instr_1 = \frac{1 - r}{1 + r} \quad (6)$$

$$d(Instr_1) = \frac{N \cdot r}{(1 + r)^2} \quad (7)$$

For detector instrumental asymmetry $Instr_2$ (again, note the different definition or “ r ”) –

$$r = \frac{L^+ R^+}{L^- R^-}$$

$$N = \sqrt{\frac{1}{L^+} + \frac{1}{L^-} + \frac{1}{R^+} + \frac{1}{R^-}}$$

$$Instr_2 = \frac{1 - r}{1 + r} \quad (8)$$

$$d(Instr_2) = \frac{N \cdot r}{(1 + r)^2} \quad (9)$$

For the Up-Down plane, simply replace all L's with U's and R's with D's in the above equations.

Analysis Code – Second Loop, Calculating Rates

In the second loop subroutine, all events recorded in a given run's ROOT tree are gone through in order to build the helicity-dependent energy spectra. At this time, outside of our cuts, we sum several scalers to be used in rate calculations – the BCM VtoF scaler is used to calculate current I , after being cross-calibrated against BCM 0L02; the detector trigger scaler $N_{triggers}$ and the accepted triggers scaler $N_{accepted}$ to be used in calculating the a DAQ deadtime correction; and the 121 kHz clock scaler to be used to calculate the run time T . We also sum detector-specific dE rate scalers that when multiplied by our coincidence window $\tau_{coincidence}$ are used to calculate unique detector electronics deadtime corrections. Inside of our cuts, during this pass through the raw scalers, we record the number N of “good” scatterings from the target foil per detector, helicity-independent. From these quantities, the rate and uncertainty for a given detector can be calculated as –

$$R_{LRUD}[Hz/\mu A] = \frac{N_{LRUD}}{T[s] \cdot I[\mu A]} \cdot \frac{N_{triggers}}{N_{accepted}} \cdot \frac{1}{1 - ((R_{dE})_{LRUD}[Hz] \cdot \tau_{coincidence}[s])} \quad (10)$$

$$dR_{LRUD}[Hz/\mu A] = R_{LRUD} \sqrt{\frac{1}{N_{LRUD}} + \frac{1}{N_{triggers}} + \frac{1}{N_{accepted}} + \left(\frac{dI}{I}\right)^2 + \left(\frac{dT}{T}\right)^2} \quad (11)$$

$N_{triggers} / N_{accepted}$ is our DAQ deadtime correction, common to all four detectors. This correction can be as large as 1.2 when running on the 1 micron foil, and is less for thinner foils – the thicker the

foil, the larger the rate and thus the DAQ deadtime. The error contribution from this quantity is expressed by $(N_{triggers})^{-1}$ and $(N_{accepted})^{-1}$. These quantities are usually on the order of millions and so their error contribution is small, $\sim 10^{-6}$.

$(1 - (R_{dE})_{LRUD} * \tau_{coincidence})^{-1}$ is our detector-dependent electronics deadtime correction.

$\tau_{coincidence}$ is the coincidence window between E and dE detectors, 100ns, set in hardware. $(R_{dE})_{LRUD}$ is typically $\sim 10^5$ Hz, and so the correction is typically unity until the third decimal place. The error contribution from this quantity is at most 10^{-7} , and so we do not include it.

Run time T is calculated from our 121 kHz clock –

$$\text{RunTime } T \text{ [s]} = \text{clock_scaler} / \text{clock_rate [Hz]} \quad (12)$$

Our 121 kHz clock rate was measured to be 121340.0 Hz, with a drift of as much as 100 Hz. From this, we determined $dT = 100 / 121340 = 8.241E-04$.

Electron beam current I, on the order of microamps, is calculated from a BCM scaler that is cross-calibrated against BCM 0L02. This is done by plotting BCM scaler values versus BCM 0L02's readback and fitting the data with a line from which a slope/gain m and intercept/offset b, along with uncertainties, is determined. Then, beam current I and uncertainty σ_I can be calculated as –

$$I [\mu A] = \frac{1}{m} \cdot \left(\frac{BCM_{scaler}}{T} - b \right) \quad (13)$$

$$\sigma_I [\mu A] = \sqrt{\frac{1}{m^2 T^2} \cdot \left[S + T^2 \sigma_b^2 + T^2 I^2 \sigma_m + \frac{S^2}{T^2} \sigma_T \right]} \quad (14)$$

This was done for both Runs I and II respectively, using all times Mott data was being acquired (ie anytime the Mott Run Number PV was non-zero, indicating the DAQ as recording). This cross-calibration against BCM 0L02 means our current is known only to the accuracy of BCM 0L02. No absolute calibration of BCM 0L02 was done in either Run I or II, and so we do not speak of *absolute* rates when we talk about them, rather we are speaking of *relative* rates.

Since in practice we take multiple runs on the same foil and then average them together, averaging rates and asymmetries, and in order to not treat our beam current quantity in the rates calculation as a statistical one, the analysis code reports rates in units of Hz, calculated by

$$R_{LRUD} [Hz] = \frac{N_{LRUD}}{T [s]} \cdot \frac{N_{triggers}}{N_{accepted}} \cdot \frac{1}{1 - ((R_{dE})_{LRUD} [Hz] \cdot \tau_{coincidence} [s])} \quad (15)$$

and then dR_{LRUD} becomes –

$$dR_{LRUD}[Hz] = R_{LRUD}[Hz] \sqrt{\frac{1}{N_{LRUD}} + \frac{1}{N_{triggers}} + \frac{1}{N_{accepted}} + \left(\frac{dT}{T}\right)^2} \quad (16)$$

Current I and uncertainty σ_I are then used outside of the analysis code to calculate final relative rates and uncertainties in Hz/uA.

Analysis Code – Scaler Loop

In the scaler loop subroutine of the analysis code, scalers for BCM VtoF, helicity, and pattern synchronization are used in order to calculate charge asymmetry. For Runs I and II, the CEBAF helicity control board was configured to produce a quartet helicity pattern – either “- + + -” or “+ - - +” – with each helicity state lasting for 33330 us, or helicity changes at a frequency of roughly 30Hz. The pattern synchronization logic scaler – a square wave with high or low value – is used to determine whether a quartet has begun, or not, in realtime. Logic scaler T_settle is recorded with every Mott event. T_settle monitors the Pockels cell used to flip helicity, and if the cell is changing it will read high, indicating ambiguous helicity state and thus flagging the event as unusable. The BCM VtoF scaler is used to determine that the electron beam is indeed on and what current is being sent in counts. Of our two sets of scalers S1 (or Ring) and S2, S1 is helicity-gated, and so it is used for the charge asymmetry calculation. Since it only reads when helicity is well-defined we do not have to account for T_settle in this loop.

When a quartet is determined to have begun and beam is on, the next four helicity states' current in counts from BCM VtoF scaler are recorded, quantities q_1, q_2, q_3, q_4 . Then, the charge asymmetry for that quartet is calculated as the difference between positive and negative helicities over the sum of all helicities. That is, if q_1 is positive helicity, then charge asymmetry for the quarter A_q is –

$$A_q = \frac{(q_1 + q_4) - (q_2 + q_3)}{(q_1 + q_4 + q_2 + q_3)} \quad (17)$$

and if q_1 is negative helicity –

$$A_q = \frac{(q_2 + q_3) - (q_1 + q_4)}{(q_1 + q_4 + q_2 + q_3)} \quad (18)$$

Values of A_q are then added to a histogram after being converted to parts per million. Figure 16 shows

run 8545's charge asymmetry histogram. This histogram is comprised of 200 bins from -10000 to 10000 ppm. Data is shown in blue. The data is then fit with a Gaussian shown in green, again using ROOT's default TH1 fitter, a χ^2 function minimized using Minuit and the MIGRAD minimizer. The seed-value for the mean of the fit was chosen to be zero, since that would be the ideal case, while the amplitude seed value of 1000 and the sigma seed value of 10000 were chosen heuristically.

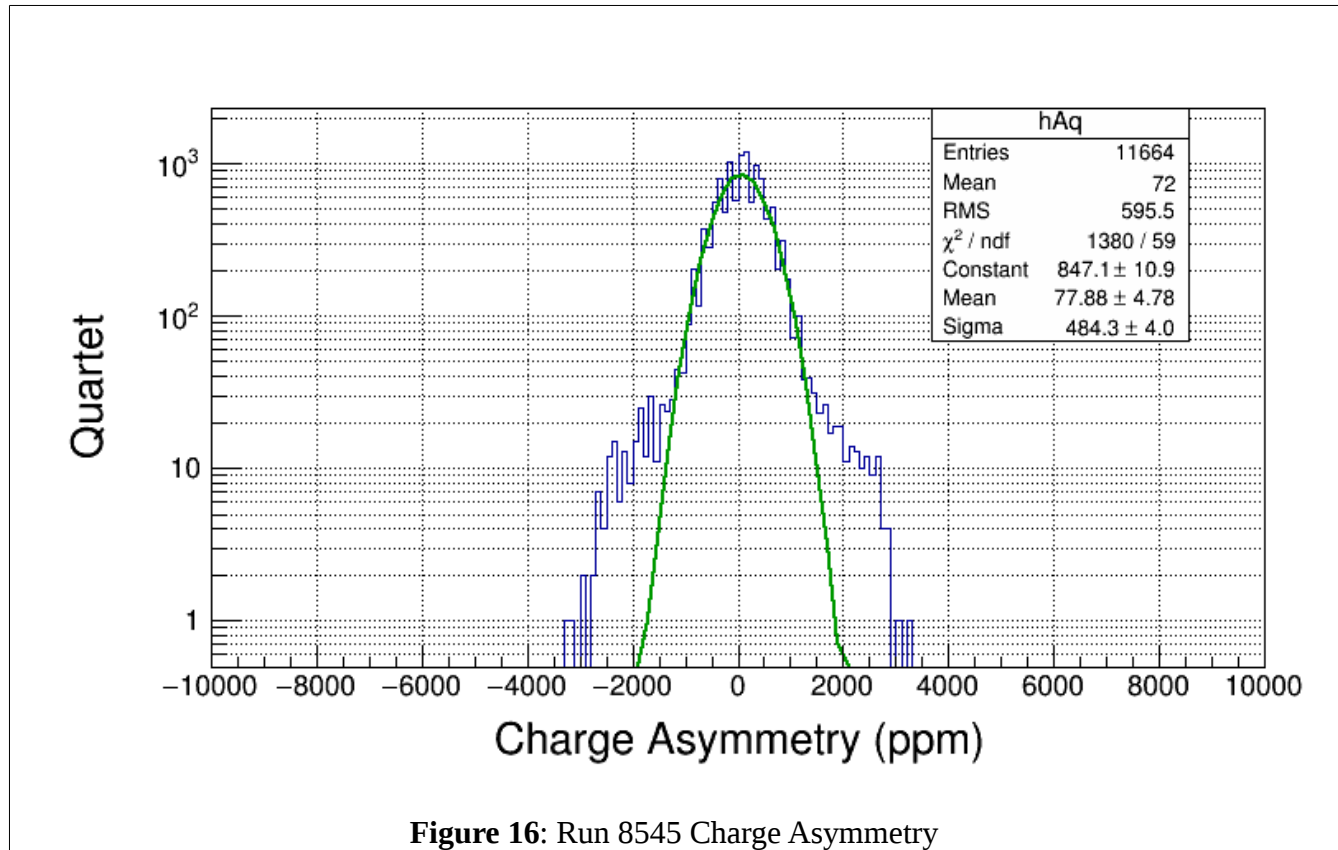


Figure 16: Run 8545 Charge Asymmetry

The fit is used to compare with the data and qualitatively assess how close to Gaussian the data distributes itself. The charge asymmetry for a given Mott data run in ppm is the mean of the histogram (not the fit's), with uncertainty equal to the root-mean-squared divided by the square root of the number of entries.

Choice of Cuts – Time-of-Flight Cuts

Time-of-flight spectra for each Left, Right, Up and Down detector are the first data fit in the analysis code. This is done with a Gaussian fit in the range of 49 to 55 ns, where we observe our scatterings from the target foil from each detector. This range was chosen because it easily encompasses all four detectors' ToF target scatterings peaks. These peaks, as shown in Figure 17, run 8545's ToF Spectra fit with Gaussians, do not necessarily occur at the exact same time for each detector – Left detector ToF target peak occurs at 53.81 ns, Right at 53.37 ns, Up at 53.40 ns, and Down at 53.21 ns. These differences can be attributed to slight differences in cabling for each detector.

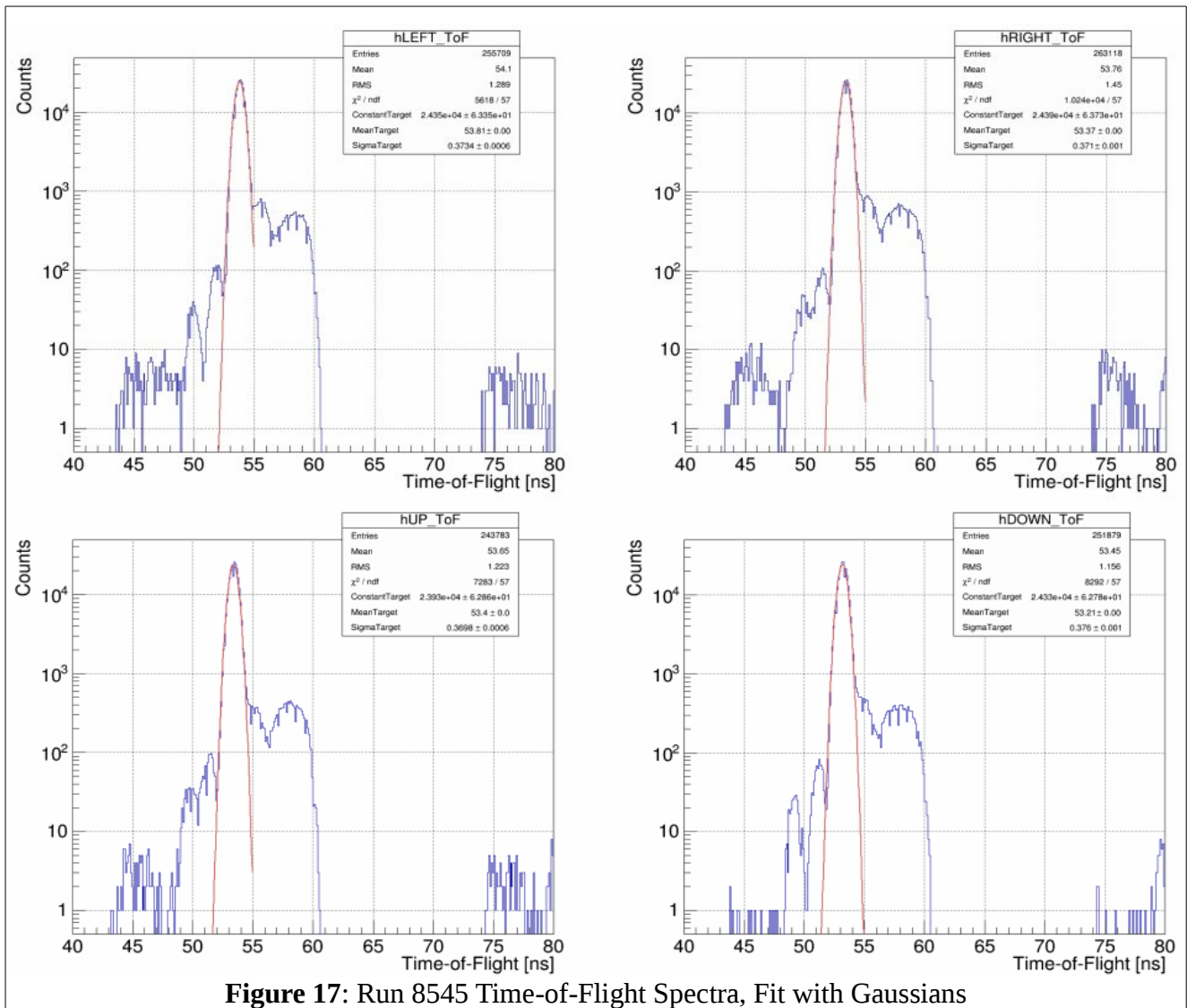


Figure 17: Run 8545 Time-of-Flight Spectra, Fit with Gaussians

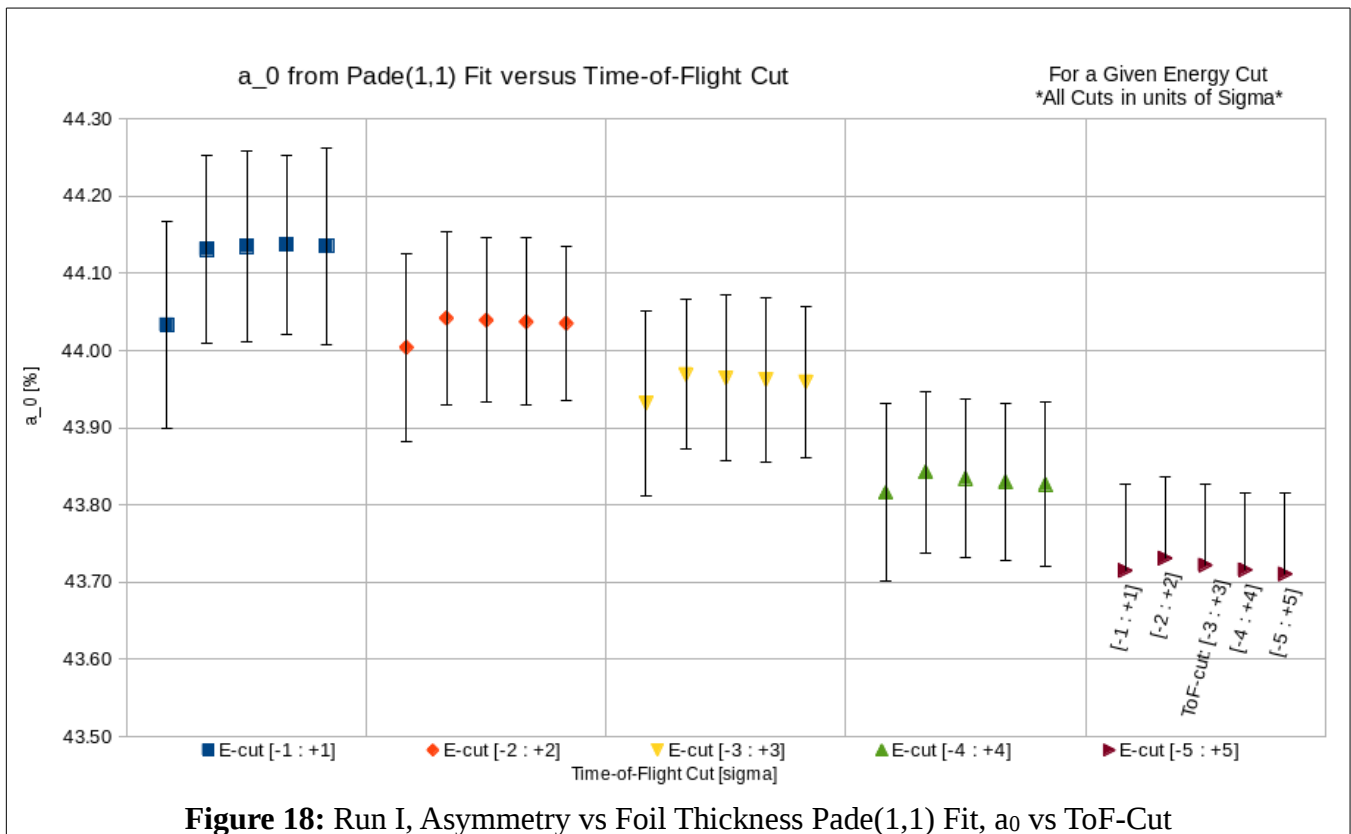
In keeping with a reproducible, methodical approach that will work for every Mott run where a ToF cut can be employed – runs where the beam repetition rate is setup appropriately – we then use the

results of the Gaussian fits to determine a ToF-cut for each detector. Defining the ToF-cut range as multiples of sigma about the mean of each of these fits we account for differences in detector temporal resolutions. The exact multiple of sigma, ± 2 , was determined by observing the effects of widening and narrowing this cut range had on the the fit parameters of the final Asymmetry versus Foil Thickness fit. Two different Asymmetry vs Foil Thickness fits were considered – the simulation-predicted fit (see Reference [3] M.J. McHugh, "GEANT4 Simulation of the Jlab MeV Mott Polarimeter"), a Pade(1,1) form shown in Equation 19, and the next best Pade fit form based on reduced χ^2 s of all fits tried, a Pade(0,1) form shown in Equation 20. For detailed discussion of Pade fitting, see Reference [2] M. L. Stutzman, D. G. Moser, T. J. Gay, "Extrapolation of Asymmetry Data to Determine A_0 ."

$$A(t) = \frac{a_0 + a_1 t}{1 + a_2 t} \tag{19}$$

$$A(t) = \frac{a_0}{1 + a_1 t} \tag{20}$$

Different ToF-cut ranges were considered for a given energy cut, observing how they affected the resulting fit parameters. In particular, the parameter of interest in either fit form is the zero-thickness asymmetry a_0 (in some places labeled A_0), as it is a direct measure of the polarimeter's analyzing power and precision. Figure 18 displays a_0 from the Pade(1,1) fit versus ToF-cut range, using Run I data.



Each color group of data points in Figure 21 represent a given Energy cut range, with five ToF-cut ranges from ± 1 sigma about the mean up to ± 5 sigma, sequentially from left to right. For Energy cut ± 5 sigma, the negative portion of the error bar on a_0 was omitted for the data label, but can be imagined as exactly the same magnitude as the positive portion. From this, we conclude that for a given Energy cut varying the ToF-cut range does not affect the a_0 parameter of the Pade(1,1) fit, except for in the ± 1 sigma ToF-cut range case, where a_0 is made slightly less, but still within the uncertainty of all other cases. a_0 certainly exhibits dependence on choice of Energy cut, however.

For completeness, the dependence of a_1 and a_2 on ToF-cut range choice is shown in Appendix XX along with a table of all Pade(1,1) fit parameters versus ToF-cut and the reduced χ^2 s and probabilities of the fits.

Next, we consider the Pade(0,1) fit form and how its parameters are affected by changing the ToF-cut range. Figure 19 shows how the a_0 parameter from the Pade(0,1) is affected by choice of

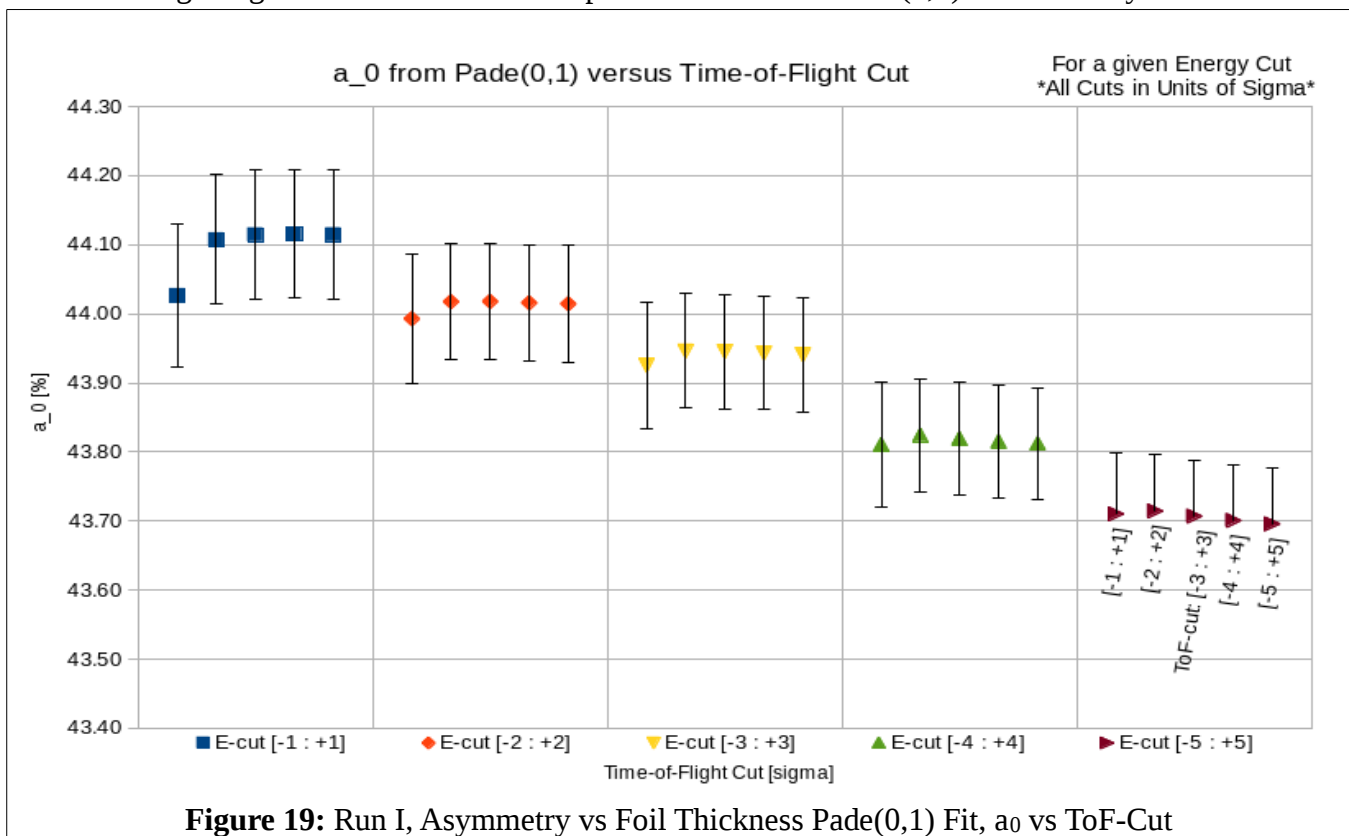
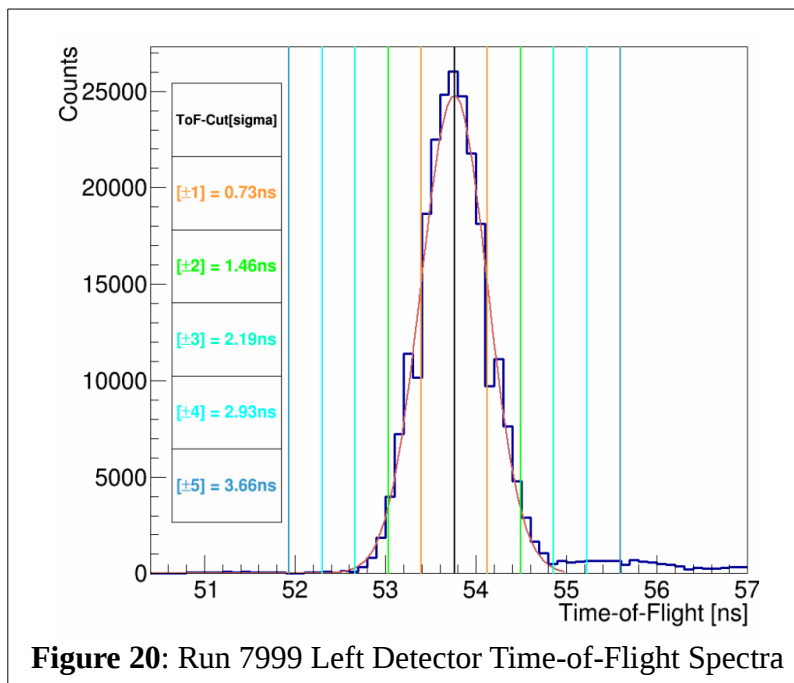


Figure 19: Run I, Asymmetry vs Foil Thickness Pade(0,1) Fit, a_0 vs ToF-Cut

ToF-cut range for various energy cuts. Again, we see little dependence of a_0 on choice of ToF-cut range for a given energy cut, although we do see a dependence on energy cut. ToF-cut range ± 1 produces, again, an a_0 value slightly less than all other choices, but still within the error bars of all other choices. Appendix ## presents the a_1 -parameter vs ToF-cut and a table of all fit parameters from the Pade(0,1)

fit versus ToF-cut along with reduced χ^2 s and probabilities of fits.

Based on these results for either fit form, we conclude that ToF-cut range ± 1 sigma is the only choice that should be thrown out, and ranges ± 2 to ± 5 sigma could be chosen with negligible effect on the fits. To be conservative in insuring we are only choosing events that are scatterings from the target foil and not elsewhere, we choose ± 2 sigma about the mean of our Gaussian fit of the Time-of-Flight spectra to be our standard Time-of-Flight cut. If the target scatterings peak was perfectly Gaussian, this would account for 95.45% of all target scatterings. To give a sense of magnitude in ns of this cut, Figure 20 shows run 7999's, from Run I, Left detector fit ToF-spectra. For this run, our standard ToF-cut will give us a 1.46 ns window.



To be absolutely sure ± 2 sigma about the mean is the right ToF-cut range to choose, we can observe how the fit parameters for the Asymmetry versus Foil Thickness change when using our standard Energy cut from -0.5 sigma to +2 sigma. Tables 1 and 2 present these results for Run I data and the two different fit forms, meanwhile 3 and 4 show Run II data. Identical to within an error bar results with this Energy Cut, even from Run I to II, so no reason to change our standard ± 2 sigma about the mean ToF-cut.

Run I Asymmetry vs Thickness Pade(0,1) Fit Parameters					
Energy Cut [E-fit sigma]	ToF Cut [ToF-fit sigma]	a_0	$d(a_0)$	a_1	$d(a_1)$
[-0.5 : +2]	[-1 : +1]	44.04	0.10	0.315	0.009
[-0.5 : +2]	[-2 : +2]	44.08	0.09	0.316	0.008
[-0.5 : +2]	[-3 : +3]	44.08	0.09	0.317	0.008
[-0.5 : +2]	[-4 : +4]	44.09	0.09	0.317	0.008
[-0.5 : +2]	[-5 : +5]	44.08	0.09	0.317	0.008

Table 1

Run I Asymmetry vs Thickness, Pade(1,1) Fit Parameters							
Energy Cut [E-fit sigma]	ToF Cut [ToF-fit sigma]	a_0	$d(a_0)$	a_1	$d(a_1)$	a_2	$d(a_2)$
[-0.5 : +2]	[-1 : +1]	44.06	0.13	0.986	3.917	0.343	0.112
[-0.5 : +2]	[-2 : +2]	44.11	0.12	1.428	3.808	0.357	0.108
[-0.5 : +2]	[-3 : +3]	44.11	0.12	1.263	3.905	0.353	0.111
[-0.5 : +2]	[-4 : +4]	44.11	0.12	1.266	3.772	0.353	0.107
[-0.5 : +2]	[-5 : +5]	44.11	0.12	1.270	3.928	0.353	0.112

Table 2

Run II Asymmetry vs Thickness Pade(0,1) Fit Parameters					
Energy Cut [E-fit sigma]	ToF Cut [ToF-fit sigma]	a_0	$d(a_0)$	a_1	$d(a_1)$
[-0.5 : +2]	[-1 : +1]	44.01	0.11	0.311	0.009
[-0.5 : +2]	[-2 : +2]	44.08	0.10	0.314	0.009
[-0.5 : +2]	[-3 : +3]	44.08	0.10	0.314	0.009
[-0.5 : +2]	[-4 : +4]	44.08	0.10	0.314	0.009
[-0.5 : +2]	[-5 : +5]	44.08	0.10	0.314	0.009

Table 3

Run II Asymmetry vs Thickness, Pade(1,1) Fit Parameters							
Energy Cut [E-fit sigma]	ToF Cut [ToF-fit sigma]	a_0	$d(a_0)$	a_1	$d(a_1)$	a_2	$d(a_2)$
[-0.5 : +2]	[-1 : +1]	44.07	0.15	3.146	4.607	0.399	0.131
[-0.5 : +2]	[-2 : +2]	44.14	0.14	3.727	4.521	0.419	0.128
[-0.5 : +2]	[-3 : +3]	44.14	0.13	3.802	4.416	0.421	0.125
[-0.5 : +2]	[-4 : +4]	44.15	0.14	3.824	4.841	0.422	0.137
[-0.5 : +2]	[-5 : +5]	44.14	0.13	3.823	4.545	0.422	0.128

Table 4

Choice of Cuts – Energy Cuts

After determining and applying our Time-of-Flight cuts for each detector, if they are employed, to our data we are left with energy spectra that are then horizontally normalized and fit with Gaussians. From these fits, an energy cut is defined as between -0.5 and +2 sigma. We arrived at our choice of energy cut by studying the effect each half-sigma-wide energy cut 'slice' from -5 to +5 sigma about the mean had on the resulting Asymmetry versus Foil Thickness fit parameters. In other words, we considered energy spectra slices from -5 sigma to -4.5 sigma, -4.5 to -4, and so on up to +5 sigma, individually, calculating each slice's asymmetry for each foil thickness, and then fitting the asymmetry versus foil thickness data per slice. Two fits, again, were considered — a Pade(1,1), Equation 19, that is predicted from simulation, and the next best fit form, a Pade(0,1), Equation 20.

$$A(t) = \frac{a_0 + a_1 t}{1 + a_2 t} \quad (19 \text{ duplicate})$$

$$A(t) = \frac{a_0}{1 + a_1 t} \quad (20 \text{ duplicate})$$

Again, the parameter of greatest interest is a_0 . Its variation versus energy slice, for Run I and II data, is displayed in Figures 21 for Pade(0,1) and 22 for Pade(1,1). Each data point sits in the center of the energy slice considered. (e.g. energy slice +2 to +2.5 sigma sits at +2.25 on the x-axis)

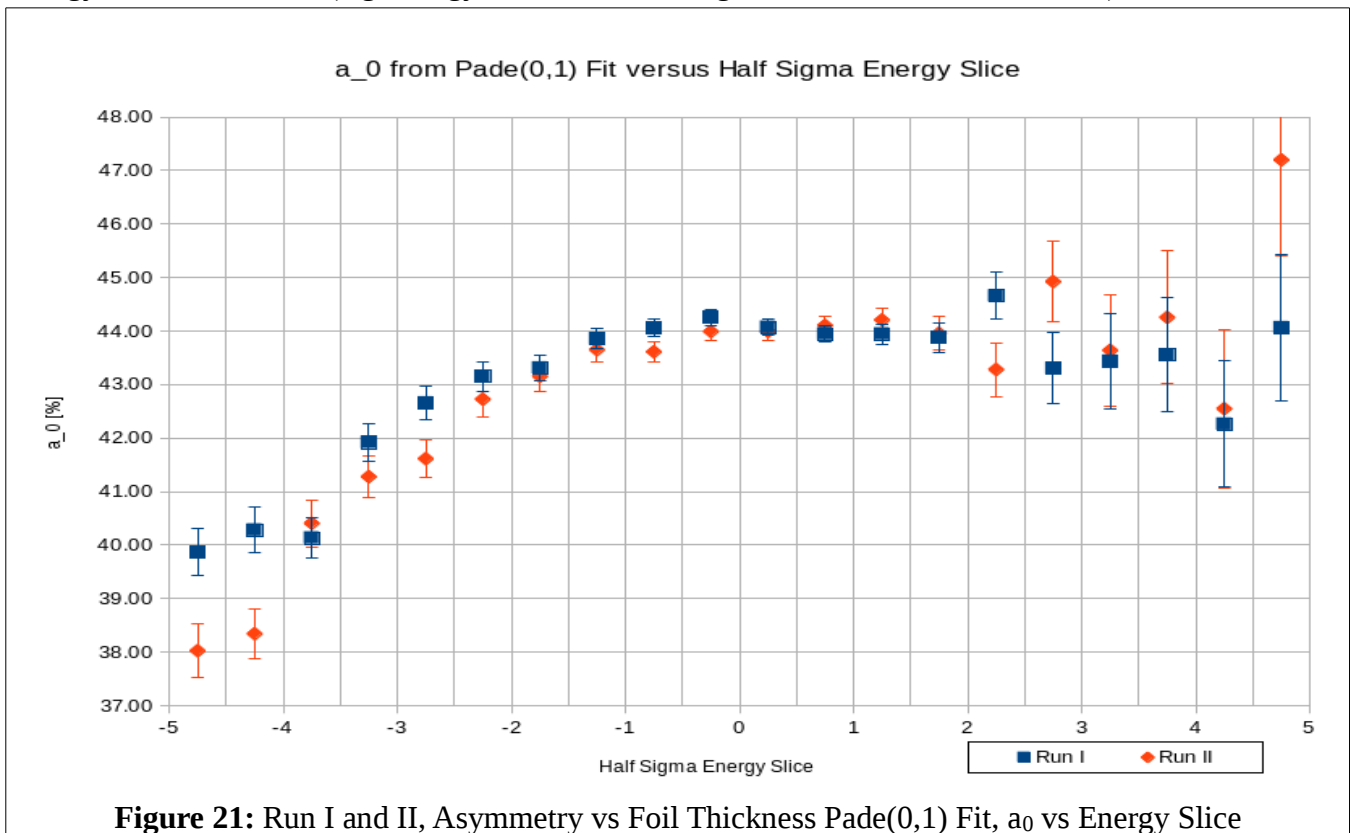
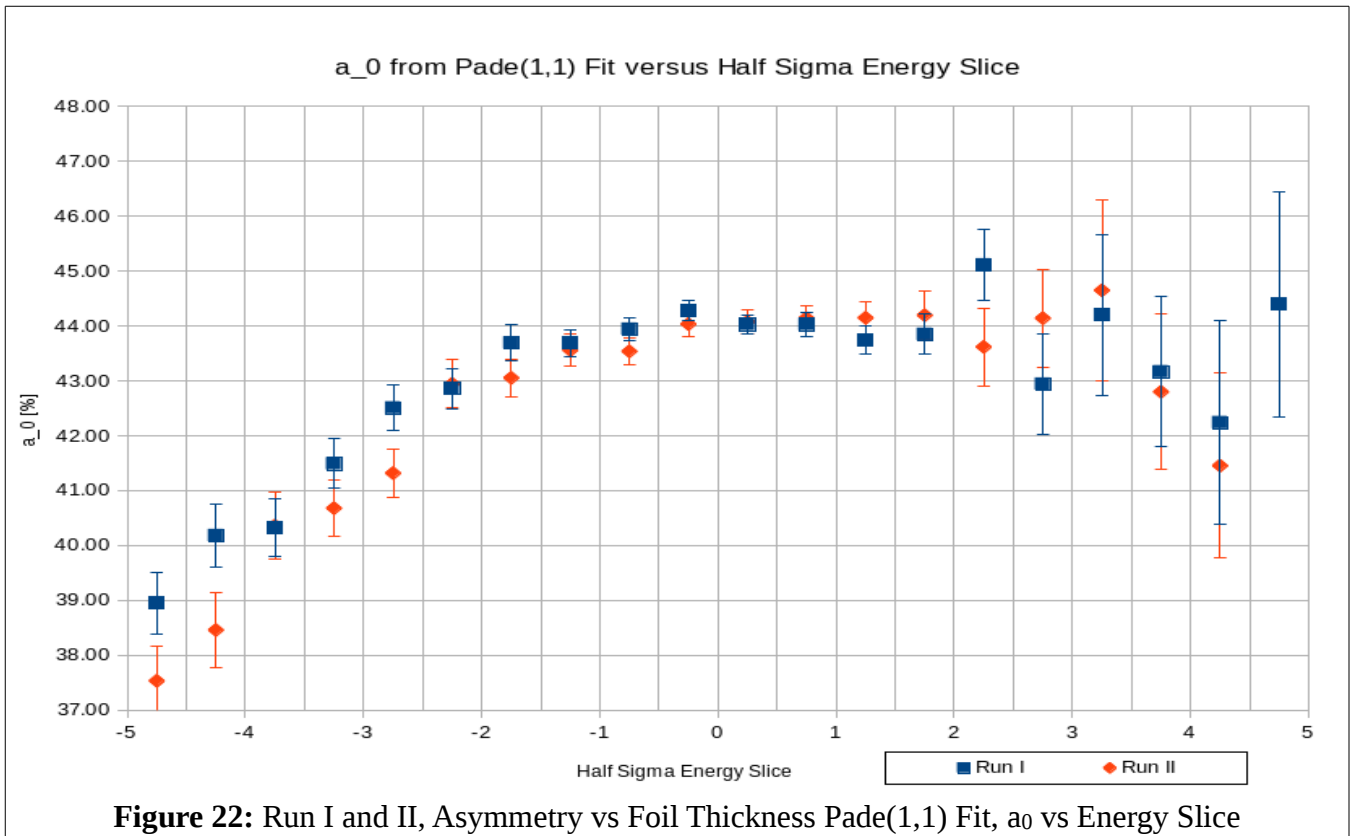


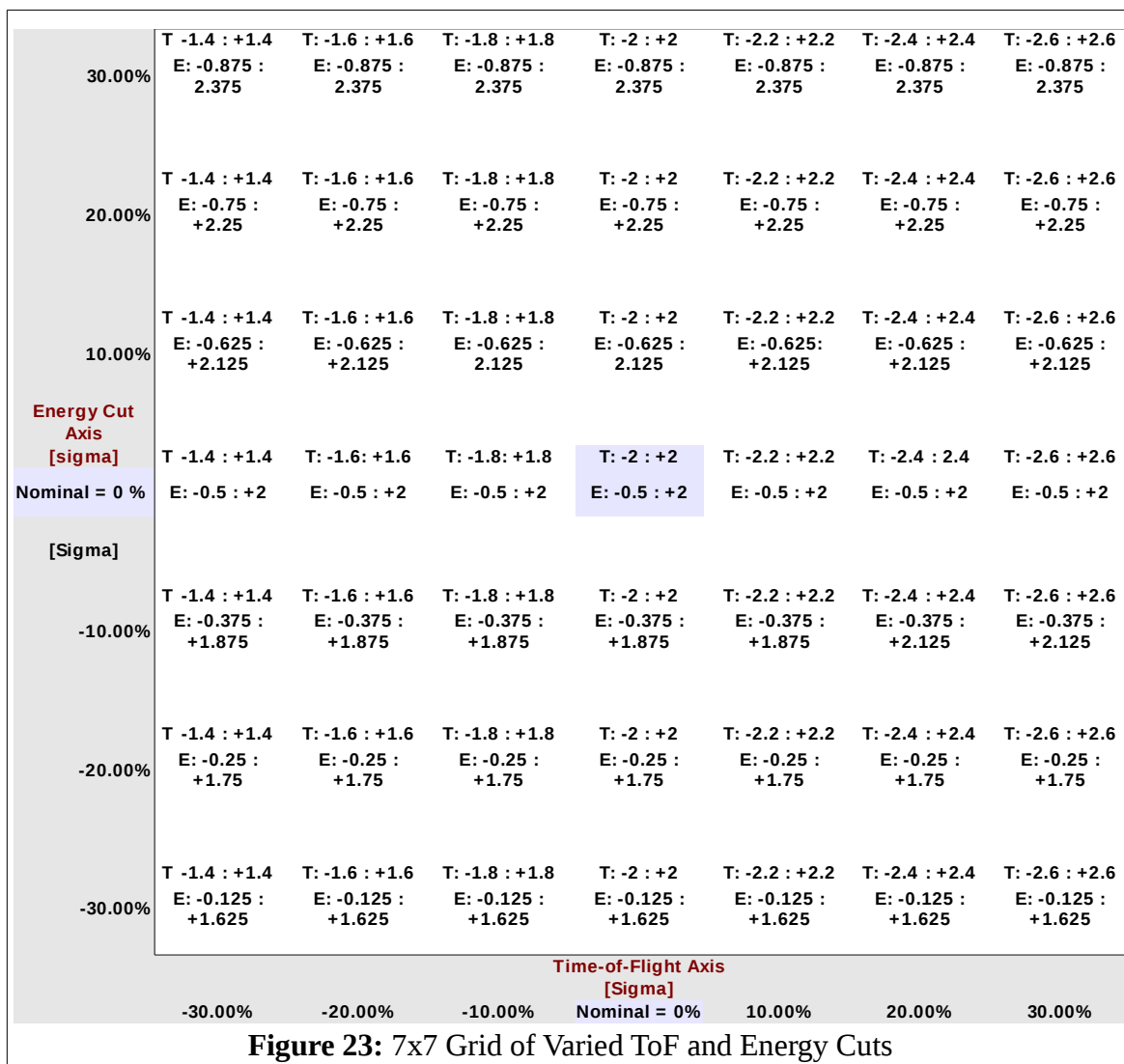
Figure 21: Run I and II, Asymmetry vs Foil Thickness Pade(0,1) Fit, a_0 vs Energy Slice



To minimize analyzing power dilution, we choose the largest a_0 values, which as one would expect, occur closest to the mean. At the same time, we strive to keep our uncertainty as small as possible, and so we exclude points of large uncertainty from consideration. With these stipulations, we arrive at our choice of -0.5 sigma to $+2$ sigma as our energy cut – a_0 is maximized and consistent across this range with the least uncertainty, for both Runs I and II.

Sensitivity to Choice of Cuts

One run was chosen from each set of runs on a given foil thickness from the Asymmetry vs Foil Thickness studies, and then an additional run from each set of stability runs – Run I has two sets of stability runs, one with the low-threshold PMT setting, one with the high-threshold PMT settings; Run II has only one set of stability runs; all stability runs are on the 1 micron foil. Run I's sample set, then, has 12 individual runs, Run II's has 11. These runs were then run through the analysis code with various Time-of-Flight and Energy cuts, about our nominal ones – ToF: -2 to +2 sigma; E: -0.5 to +2 sigma. 10% steps of the nominal Time-of-Flight and Energy Cut windows were chosen, varying each by as much as +/- 30%, and creating a 7x7 grid of results as shown in Figure 23.



Two grids were created – one for the physics asymmetry and one for the average rate.

Sensitivity to Choice of Cuts – Asymmetry Grid

With a correct choice of nominal cuts we expect nearly all of the events encompassed by our cut area on an Energy vs ToF 2D plot, Figure 13, to be from scatterings off of the target foil and carrying asymmetry. Varying these cuts by as much as +30% this assumption should remain true, and of course it is true when shrinking our cut area. As such, we can directly compare asymmetries computed using our nominal set of cuts to asymmetries computed using varied cuts. This is done by dividing the varied-cut asymmetry for a given foil thickness by the corresponding nominal-cut asymmetry for the same foil, creating an asymmetry ratio.

$$\text{Asymmetry Ratio} = A(\text{varied-cuts}) / A(\text{nominal-cuts}) \quad (21)$$

Then, for each set of varied cuts, the average and the standard deviation (standard deviation of a sample) of the asymmetry ratios was computed. The take-away is the standard deviation of a varied set of cuts' asymmetry ratios. This value is a direct measure of the amount of change in physics asymmetry due to change from nominal cuts. If a varied set of cuts produced the exact same asymmetries as the nominal set, this value would be zero. The more the asymmetries computed from a varied set of cuts vary from the nominal set of cuts asymmetries, the larger this value will be.

From these standard deviations, Table 5 is created from Run I data. The center box with blue-grey background represents nominal cuts, or 0% variation in cuts. The 8 values around it, represent the 10% variation in cuts box, with the next encompassing box being the 20% variation in cuts box, and then all the values the 30% variation in cuts box.

	%	T -1.4 : +1.4	T: -1.6 : +1.6	T: -1.8 : +1.8	T: -2 : +2	T: -2.2 : +2.2	T: -2.4 : +2.4	T: -2.6 : +2.6
		-30	-20	-10	0	10	20	30
E: -0.875 : 2.375	30	0.0021	0.0022	0.0023	0.0019	0.0025	0.0024	0.0026
E: -0.75 : +2.25	20	0.0019	0.0020	0.0021	0.0016	0.0022	0.0020	0.0022
E: -0.625 : +2.125	10	0.0021	0.0017	0.0018	0.0014	0.0019	0.0018	0.0020
E: -0.5 : +2	0	0.0024	0.0016	0.0015	0.0000	0.0009	0.0008	0.0011
E: -0.375 : +1.875	-10	0.0029	0.0024	0.0018	0.0014	0.0014	0.0014	0.0017
E: -0.25 : +1.75	-20	0.0037	0.0034	0.0029	0.0030	0.0027	0.0030	0.0032
E: -0.125 : +1.625	-30	0.0040	0.0033	0.0029	0.0027	0.0025	0.0025	0.0026

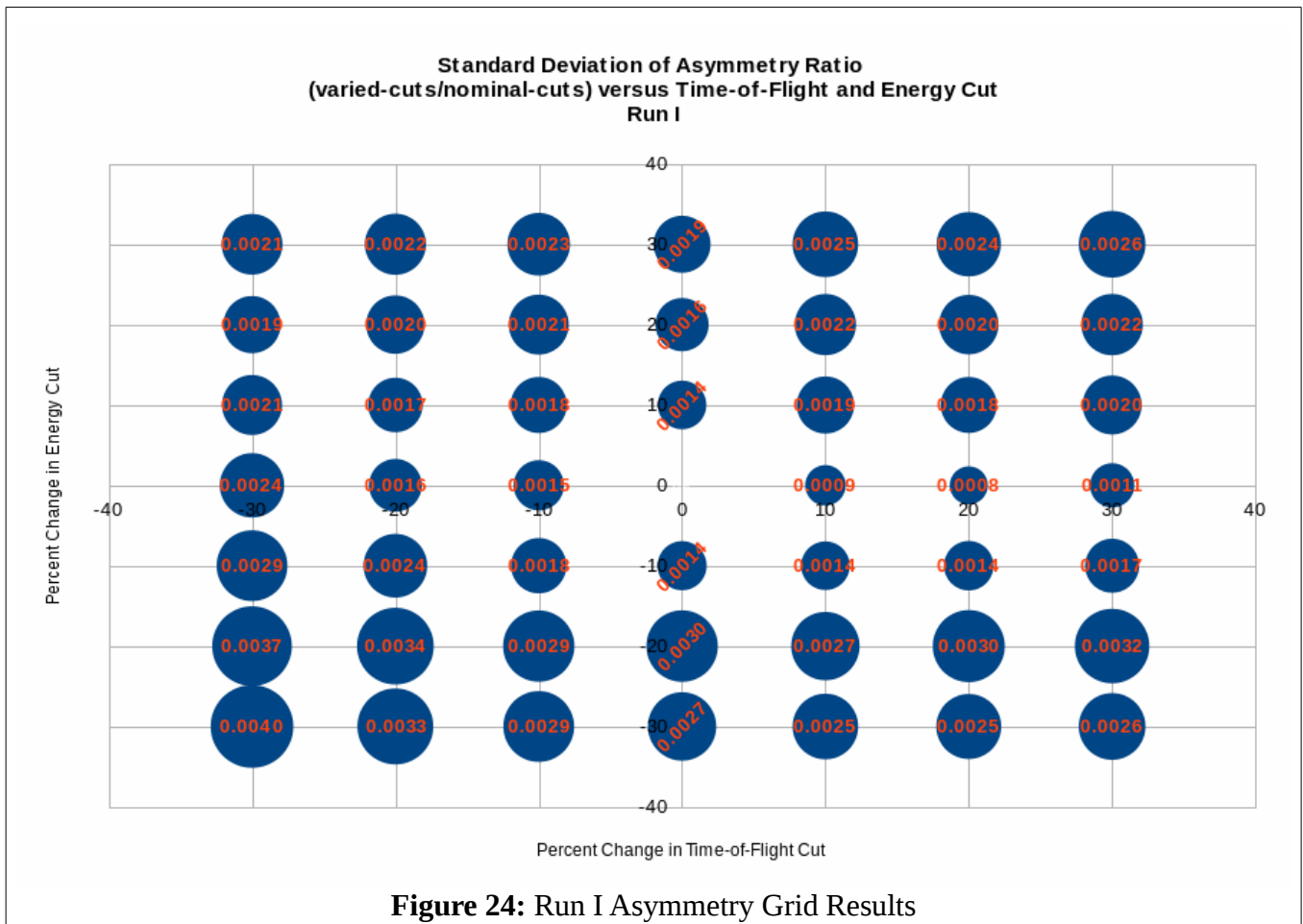
Table 5

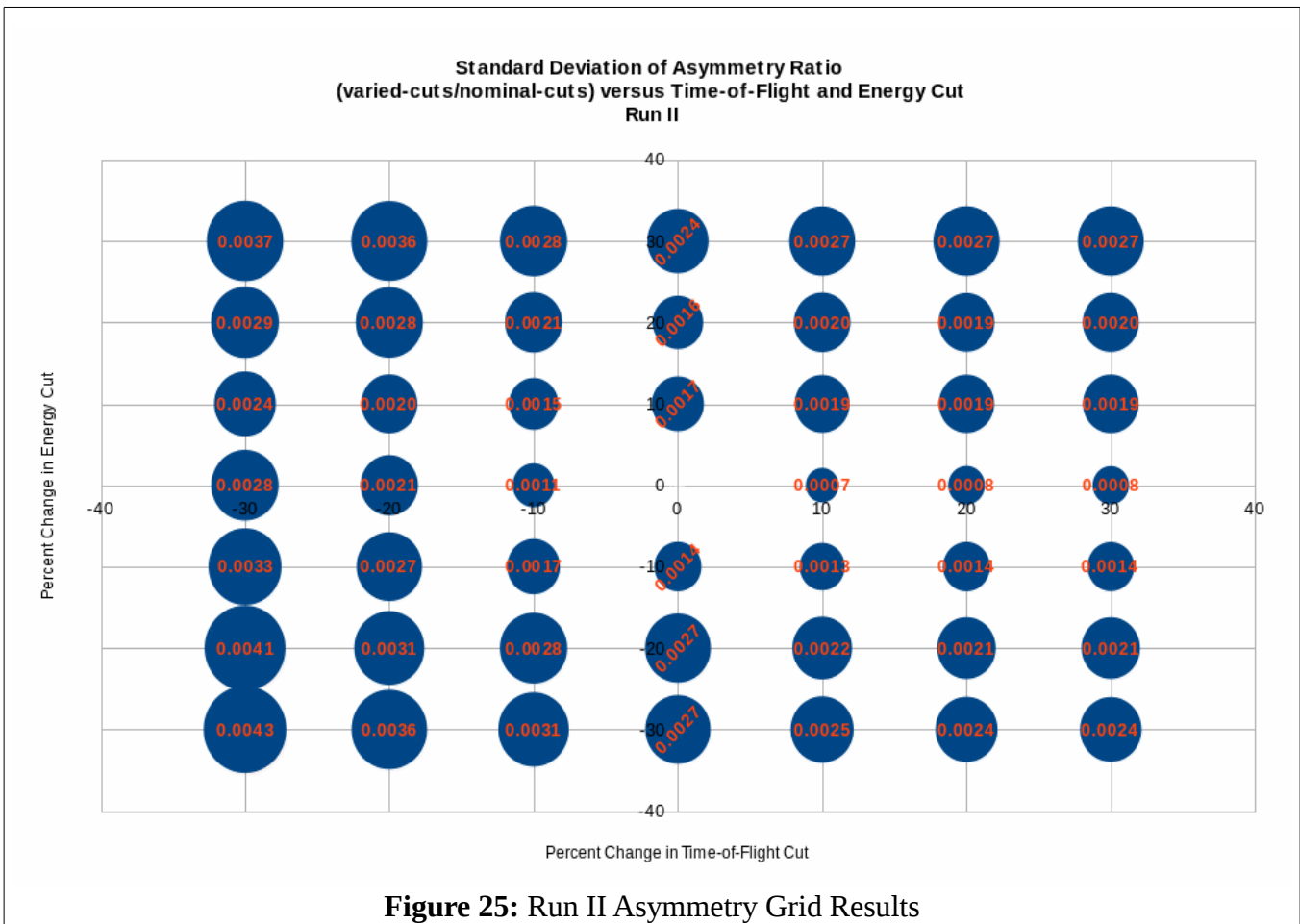
The maximum value within a given percent variation in cuts box is the maximum change in physics asymmetry due to variation in cuts up to that percent. In other words, the maximum value in a given box is a systematic uncertainty due to our choice of nominal time-of-flight and energy cuts. When multiplied by 100, this value is a percent uncertainty, as shown in Table 6 for Run I and II data.

Variation in Cuts	dA_syst_cuts	
	Run I	Run II
10 Percent Box	0.19%	0.19%
20 Percent Box	0.34%	0.31%
30 Percent Box	0.40%	0.43%

Table 6

Figures 24 and 25 show bubble charts for Runs I and II, respectively, of the standard deviation of the asymmetry ratio versus time-of-flight and energy cut variation. The axes are in percent, and the data label is the systematic percent uncertainty to asymmetry due to choice of cuts, like values in Table 6.





Sensitivity to Choice of Cuts – Average Rate Grid

A similar 7x7 grid is created for average rate. Unlike asymmetry, when varying our time-of-flight and energy cuts we expect the average rate to change because we are changing the number of good physics events used to compute asymmetry and rate in the analysis code (ie we are encompassing a smaller or larger area of the Energy vs ToF 2D plot shown in Figure 13). Rate is directly proportional to total number of good physics events, whereas asymmetry is not. To account for this, prior to filling in the 7x7 grid of average rate on a given foil for a set of cuts, we normalize each set of rates by the set's stability run and for ease of reading multiply by 100. In Run II, since all the Asymmetry vs Foil Thickness runs were taken with the same detector PMT high-voltages, all runs in our sample set are divided by the one sample stability run. In Run I, where two sets of detector PMT high-voltages were used, threshold low and high, two different stability runs are employed. If the run was performed at low threshold, it is normalized by the low threshold stability run and likewise for the

high threshold ones. The stability runs are not included in any further calculations after normalization.

Then, similar to the asymmetry grid, a ratio of stability-normalized rate is calculated for each foil in each set of varied cuts by dividing each varied-cut stability-normalized rate by the nominal-cut stability-normalized rate for a given foil thickness.

$$\text{Stability-Normalized Rate Ratio} = \frac{\text{Stability-Normalized Rate}(\text{varied cuts})}{\text{Stability-Normalized Rate}(\text{nominal Cuts})} \quad (22)$$

After this, the average and the standard deviation (of a sample) for these sets of ratios of stability-normalized rates are calculated. Again, the standard deviation is a measure of how much the stability-normalized rate changes due to variation about the nominal cuts. We construct 0, 10, 20 and 30% variation in cuts boxes, and from the maximum value in each of these boxes determine a systematic percent uncertainty due to choice of cuts on our rate. Table 7 presents results for Runs I and II.

Figures 26 and 27 show bubble charts for Runs I and II, respectively, of the standard deviation of the stability-normalized rate ratio versus time-of-flight and energy cut variation. The axes are in percent, and the data label is the systematic percent uncertainty to rate due to choice of cuts.

Variation in Cuts	dR_syst_cuts	
	Run I	Run II
10 Percent Box	0.58%	0.37%
20 Percent Box	0.68%	0.51%
30 Percent Box	0.73%	0.80%

Table 7

Standard Deviation of Stability-Normalized Rate Ratio
(varied-cuts/nominal-cuts) versus Time-of-Flight and Energy Cut
Run I

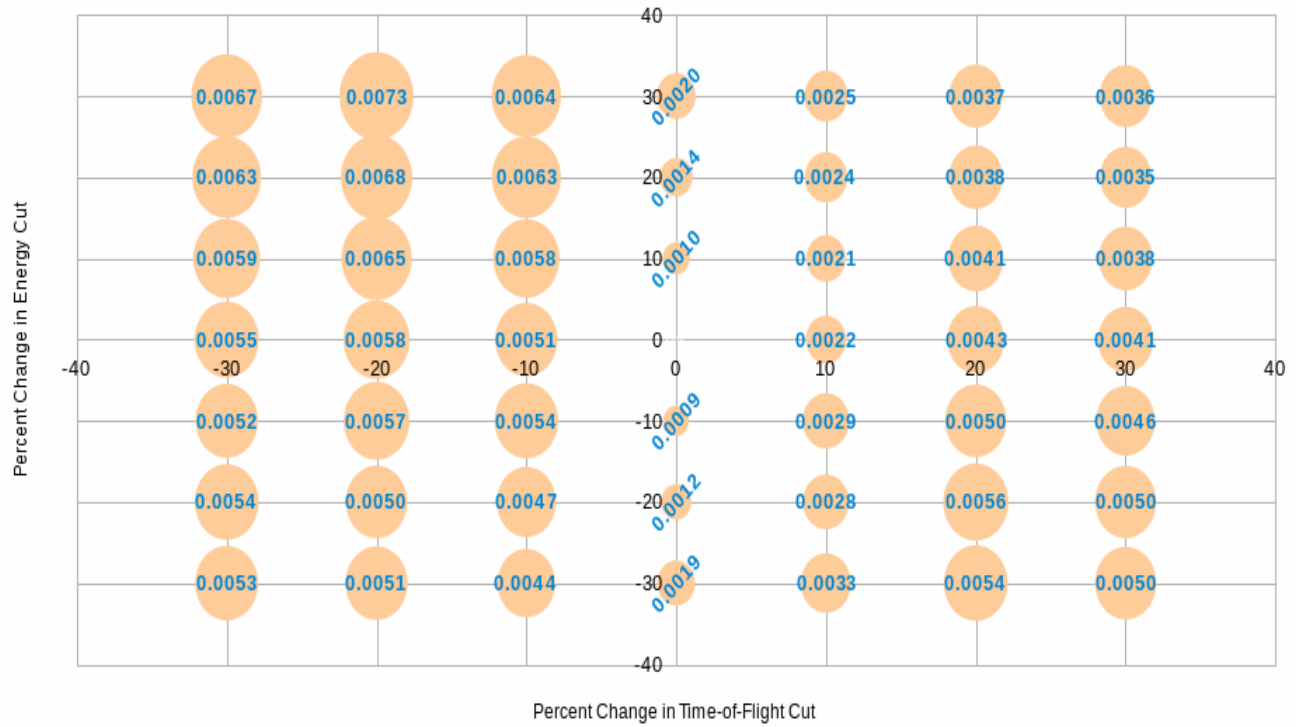


Figure 26: Run I Average Rate Grid Results

Standard Deviation of Stability-Normalized Rate Ratio
(varied-cuts/nominal-cuts) versus Time-of-Flight and Energy Cut
Run II

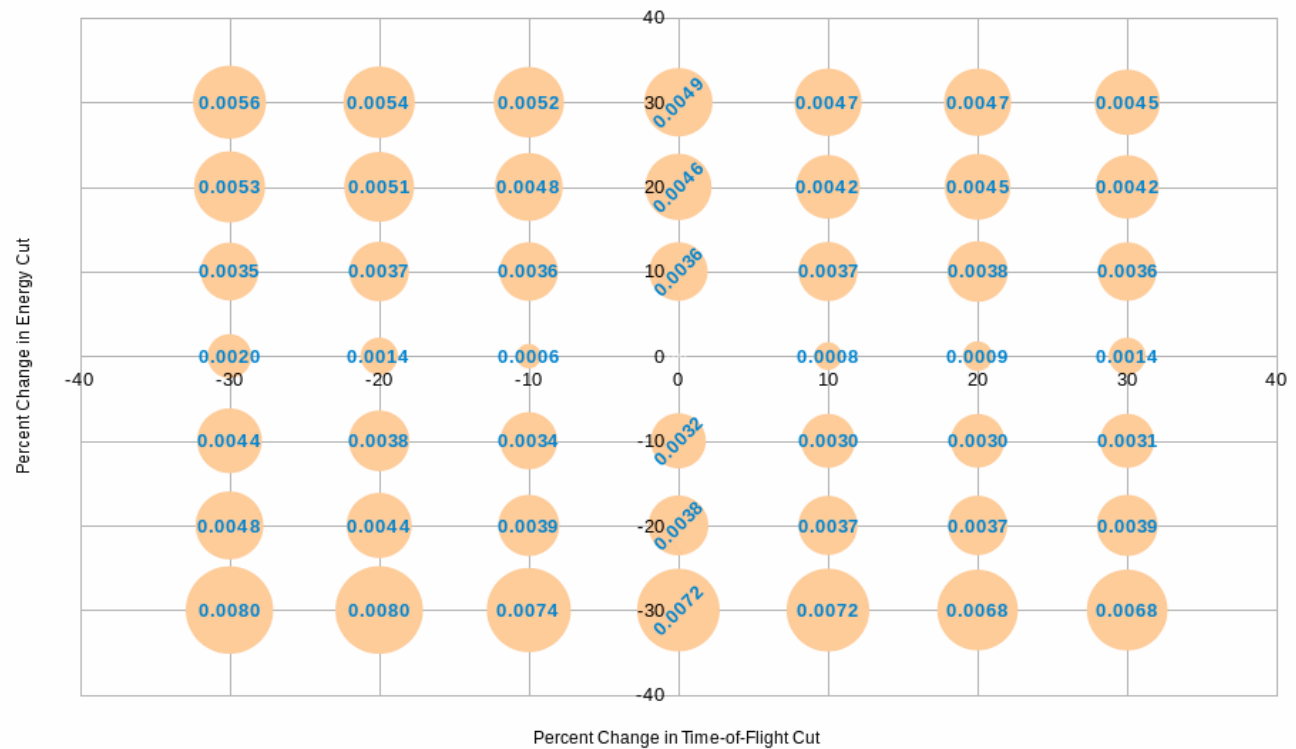


Figure 27: Run II Average Rate Grid Results

Sensitivity to Choice of Cuts – Effect on Final Fits

Table 8 presents combined asymmetry and rate results from Run I and II. The uncertainties are added in quadrature with all others for final asymmetry and rate, respectively.

Sensitivity to Choice of Cuts				
	Run I		Run II	
Variation in Cuts	dA_syst_cuts	dR_syst_cuts	dA_syst_cuts	dR_syst_cuts
10 Percent Box	0.19%	0.58%	0.19%	0.37%
20 Percent Box	0.34%	0.68%	0.31%	0.51%
30 Percent Box	0.40%	0.73%	0.43%	0.80%

Table 8

How the addition of these uncertainties affects final Asymmetry versus Foil Thickness and Asymmetry versus Average Rate was then explored.

For Asymmetry vs Foil Thickness, the three best fits are a Pade(1,1) predicted from simulation, a Pade(0,1) and then a Pade(2,0). Table 9 displays how the various fit parameters are affected by different choice of percent variation in cuts box for Run I, and Table 10 for Run II. The far left two columns refer to the simple (data – fit) = residual. Associated plots for this table, along with plots of residuals from each fit, are in the Appendix.

Run I Asymmetry vs Foil Thickness Fit Parameters' Sensitivity to Choice of Cuts											
		Fit	a0	d(a0)	a1	d(a1)	a2	d(a2)	Chi^2 / NDF	Sum of Residuals / N_points	Sum of Square of Residuals / N_points
Box (%) dA_syst_cuts	0.00%	Pade(0,1)	44.083	0.093	0.316	0.008			0.974	0.022	0.062
	0.0000	Pade(1,1)	44.109	0.118	1.428	3.808	0.357	0.108	1.066	0.012	0.065
		Pade(2,0)	44.072	0.108	-13.641	0.763	3.134	0.836	1.150	0.019	0.066
Box (%) dA_syst_cuts	10.00%	Pade(0,1)	44.073	0.110	0.315	0.009			0.815	0.015	0.062
	0.0019	Pade(1,1)	44.090	0.140	0.808	4.045	0.338	0.116	0.901	0.010	0.063
		Pade(2,0)	44.053	0.128	-13.488	0.834	2.983	0.897	0.967	0.016	0.065
Box (%) dA_syst_cuts	20.00%	Pade(0,1)	44.063	0.139	0.314	0.010			0.625	0.006	0.062
	0.0034	Pade(1,1)	44.061	0.178	-0.092	4.462	0.312	0.129	0.695	0.007	0.062
		Pade(2,0)	44.023	0.164	-13.263	0.965	2.762	1.009	0.738	0.011	0.063
Box (%) dA_syst_cuts	30.00%	Pade(0,1)	44.062	0.151	0.314	0.010			0.567	0.004	0.062
	0.0040	Pade(1,1)	44.051	0.189	-0.390	4.408	0.303	0.128	0.629	0.006	0.061
		Pade(2,0)	44.014	0.179	-13.189	1.023	2.689	1.060	0.667	0.009	0.063
Fits		Pade(0,1) ::: $A(t) = a_0 / (1 + a_1 * t)$									
		Pade(1,1) ::: $A(t) = (a_0 + a_1 * t) / (1 + a_2 * t)$									
		Pade(2,0) ::: $A(t) = a_0 + a_1*t + a_2*t*t$									

Table 9

Run II Asymmetry vs Foil Thickness Fit Parameters' Sensitivity to Choice of Cuts

		Fit	a0	d(a0)	a1	d(a1)	a2	d(a2)	Chi ² / NDF	Sum of Residuals / N_points	Sum of Square of Residuals / N_points
Box (%) dA_syst_cuts	0.00%	Pade(0,1)	44.077	0.104	0.314	0.009			1.051	0.037	0.076
	0.0000	Pade(1,1)	44.145	0.135	3.727	4.521	0.419	0.128	1.091	0.015	0.077
		Pade(2,0)	44.096	0.120	-13.892	0.796	3.548	0.879	1.195	0.022	0.079
Box (%) dA_syst_cuts	10.00%	Pade(0,1)	44.066	0.120	0.313	0.009			0.941	0.031	0.075
	0.0019	Pade(1,1)	44.131	0.155	3.271	4.701	0.405	0.133	0.995	0.013	0.076
		Pade(2,0)	44.081	0.138	-13.781	0.864	3.439	0.940	1.082	0.019	0.078
Box (%) dA_syst_cuts	20.00%	Pade(0,1)	44.054	0.141	0.312	0.010			0.811	0.023	0.075
	0.0034	Pade(1,1)	44.115	0.178	2.701	4.835	0.389	0.138	0.875	0.011	0.075
		Pade(2,0)	44.064	0.164	-13.645	0.960	3.305	1.023	0.942	0.015	0.077
Box (%) dA_syst_cuts	30.00%	Pade(0,1)	44.044	0.165	0.311	0.011			0.684	0.016	0.074
	0.0040	Pade(1,1)	44.098	0.215	2.153	5.408	0.373	0.155	0.748	0.008	0.075
		Pade(2,0)	44.047	0.195	-13.513	1.081	3.174	1.129	0.799	0.011	0.077
Fits	Pade(0,1) ::: A(t) = a0 / (1 + a1 * t)										
	Pade(1,1) ::: A(t) = (a0 + a1 * t) / (1 + a2 * t)										
	Pade(2,0) ::: A(t) = a0 + a1*t + a2*t*t										

Table 10

For Asymmetry vs Average Rate there is no simulation-predicted functional form, and so we simply observe the three best Pade fits – Pade(0,2), Pade(1,1) and Pade(2,0). Table 11 displays how the various fit parameters are affected by different choice of percent variation in cuts box for Run I, Table 12 for Run II. The residual is the same as in Tables 9 and 10, simply, residual = data – fit. Associated plots for this table, along with plots of residuals from each fit, are in the Appendix.

Run I Asymmetry vs Rate Fit Parameters' Sensitivity to Choice of Cuts

		Fit	c0	d(c0)	c1	d(c1)	c2	d(c2)	Chi^2 / NDF	Sum of Residuals / N_points	Sum of Square of Residuals / N_points
Box (%) dA_syst_cuts dR_syst_cuts	0.00%	Pade(0,2)	44.022	0.083	2.11E-03	6.08E-05	-2.79E-06	2.96E-07	1.440	0.010	0.033
	0.0000	Pade(1,1)	44.077	0.091	-9.84E-02	3.92E-03	4.34E-03	3.43E-04	1.177	0.007	0.030
	0.0000	Pade(2,0)	43.912	0.078	-8.37E-02	2.07E-03	1.62E-04	9.75E-06	2.360	0.017	0.042
Box (%) dA_syst_cuts dR_syst_cuts	10.00%	Pade(0,2)	44.016	0.106	2.11E-03	7.49E-05	-2.75E-06	3.61E-07	0.937	0.007	0.033
	0.0019	Pade(1,1)	44.072	0.116	-9.80E-02	4.85E-03	4.30E-03	4.18E-04	0.769	0.004	0.030
	0.0058	Pade(2,0)	43.903	0.099	-8.33E-02	2.54E-03	1.60E-04	1.19E-05	1.540	0.012	0.042
Box (%) dA_syst_cuts dR_syst_cuts	20.00%	Pade(0,2)	44.007	0.145	2.10E-03	9.86E-05	-2.71E-06	4.68E-07	0.541	0.004	0.033
	0.0034	Pade(1,1)	44.065	0.157	-9.75E-02	6.33E-03	4.26E-03	5.38E-04	0.445	0.003	0.030
	0.0068	Pade(2,0)	43.889	0.134	-8.28E-02	3.31E-03	1.58E-04	1.54E-05	0.893	0.008	0.042
Box (%) dA_syst_cuts dR_syst_cuts	30.00%	Pade(0,2)	44.005	0.161	2.09E-03	1.08E-04	-2.70E-06	5.11E-07	0.447	0.004	0.033
	0.0040	Pade(1,1)	44.064	0.173	-9.74E-02	6.89E-03	4.25E-03	5.84E-04	0.368	0.002	0.030
	0.0073	Pade(2,0)	43.886	0.150	-8.27E-02	3.67E-03	1.57E-04	1.70E-05	0.739	0.006	0.042
Fits	Pade(0,2) ::: A(R) = c0 / (1 + c1*R + c2*R*R)										
	Pade(1,1) ::: A(R) = (c0 + c1*R) / (1 + c2*R)										
	Pade(2,0) ::: A(R) = c0 + c1*R + c2*R*R										

Table 11

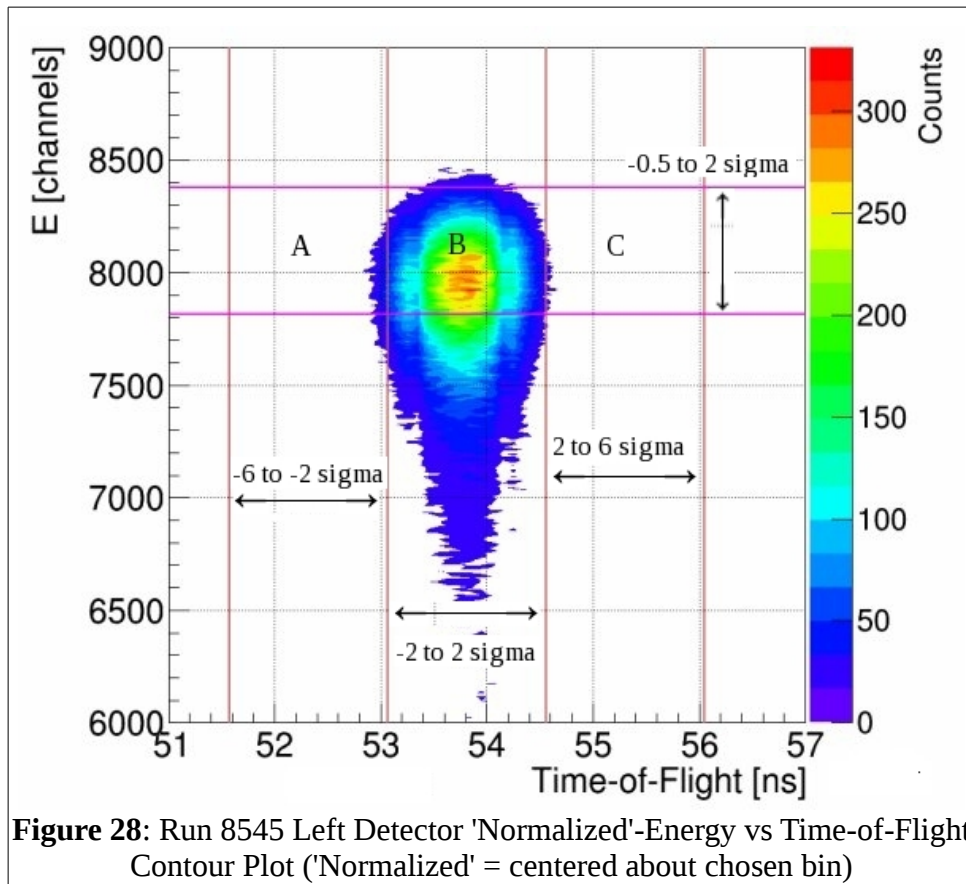
Run II Asymmetry vs Rate Fit Parameters' Sensitivity to Choice of Cuts

		Fit	c0	d(c0)	c1	d(c1)	c2	d(c2)	Chi^2 / NDF	Sum of Residuals / N_points	Sum of Square of Residuals / N_points
Box (%) dA_syst_cuts dR_syst_cuts	0.00%	Pade(0,2)	44.064	0.097	2.25E-03	7.01E-05	-3.38E-06	3.55E-07	1.505	0.010	0.040
	0.0000	Pade(1,1)	44.136	0.106	-1.06E-01	4.75E-03	4.95E-03	4.16E-04	1.218	0.007	0.036
	0.0000	Pade(2,0)	43.940	0.091	-8.82E-02	2.36E-03	1.85E-04	1.15E-05	2.451	0.016	0.051
Box (%) dA_syst_cuts dR_syst_cuts	10.00%	Pade(0,2)	44.059	0.118	2.24E-03	8.33E-05	-3.36E-06	4.20E-07	1.111	0.008	0.040
	0.0019	Pade(1,1)	44.132	0.129	-1.06E-01	5.66E-03	4.94E-03	4.92E-04	0.898	0.006	0.036
	0.0058	Pade(2,0)	43.931	0.109	-8.80E-02	2.80E-03	1.84E-04	1.37E-05	1.806	0.013	0.051
Box (%) dA_syst_cuts dR_syst_cuts	20.00%	Pade(0,2)	44.054	0.145	2.24E-03	1.02E-04	-3.34E-06	5.11E-07	0.783	0.006	0.040
	0.0034	Pade(1,1)	44.129	0.158	-1.06E-01	6.85E-03	4.92E-03	5.93E-04	0.633	0.004	0.036
	0.0068	Pade(2,0)	43.924	0.135	-8.77E-02	3.42E-03	1.83E-04	1.67E-05	1.270	0.010	0.051
Box (%) dA_syst_cuts dR_syst_cuts	30.00%	Pade(0,2)	4.051	0.178	2.23E-03	1.23E-04	-3.33E-06	6.21E-07	0.541	0.004	0.040
	0.0040	Pade(1,1)	44.127	0.193	-1.06E-01	8.25E-03	4.91E-03	7.13E-04	0.436	0.003	0.036
	0.0073	Pade(2,0)	43.918	0.164	-8.76E-02	4.13E-03	1.82E-04	2.03E-05	0.877	0.007	0.051
Fits	Pade(0,2) ::: A(R) = c0 / (1 + c1*R + c2*R*R)										
	Pade(1,1) ::: A(R) = (c0 + c1*R) / (1 + c2*R)										
	Pade(2,0) ::: A(R) = c0 + c1*R + c2*R*R										

Table 12

Background Within Our Cuts

Our cuts define an energy and time window that we deem “good” electron scatterings off of the target foil occur within. It is possible, however, for an electron to arrive in one of our detectors at the right time and with the right energy, as defined by the cuts, but not having come directly from the electron beam off of the gun cathode, and thus not with correct transverse polarization. In this case, these electrons are indistinguishable from “good” scatterings and have random polarizations, lowering or diluting our calculated physics asymmetry. Since these electrons are not coming from the gun, it is reasonable to assume they arrive at all times, and not just within our time-of-flight cut window. To estimate the amount of these diluting electrons within our cuts relative to the total number of “good” scatterings, we looked at one time-of-flight window prior to our nominal time-of-flight window, and one window after, and only electrons with energy that would make it within our energy cut. In Figure



28, region A is the one time-of-flight window before, region B our “good” scatterings region, and region C one time-of-flight window after. Then, for each detector and each region we have variables for positive and negative helicity events and their sum:

$$\begin{aligned}
L_{\{ABC\}} &= L_{\{ABC\}}^+ + L_{\{ABC\}}^- \\
R_{\{ABC\}} &= R_{\{ABC\}}^+ + R_{\{ABC\}}^- \\
U_{\{ABC\}} &= U_{\{ABC\}}^+ + U_{\{ABC\}}^- \\
D_{\{ABC\}} &= D_{\{ABC\}}^+ + D_{\{ABC\}}^-
\end{aligned} \tag{23}$$

and physics asymmetries ε for the Left-Right plane and each region, using the cross-ratio method:

$$(\varepsilon_{\{ABC\}})_{LR} = \frac{1 - \sqrt{\frac{L_{\{ABC\}}^+ R_{\{ABC\}}^-}{L_{\{ABC\}}^- R_{\{ABC\}}^+}}}{1 + \sqrt{\frac{L_{\{ABC\}}^+ R_{\{ABC\}}^-}{L_{\{ABC\}}^- R_{\{ABC\}}^+}}} \tag{24}$$

For asymmetry ε for the Up-Down plane replace Ls with Us and Rs with Ds in Equation 24. Equation 24 is simply Equation 4 with notation of region. We can also obtain an uncertainty on the asymmetry, σ_ε , from Equation 5 for each plane and region:

$$(\sigma_{\varepsilon_{\{ABC\}}})_{LR} = \frac{\sqrt{\frac{1}{L_{\{ABC\}}^+} + \frac{1}{L_{\{ABC\}}^-} + \frac{1}{R_{\{ABC\}}^+} + \frac{1}{R_{\{ABC\}}^-}} \cdot \sqrt{\frac{L_{\{ABC\}}^+ R_{\{ABC\}}^-}{L_{\{ABC\}}^- R_{\{ABC\}}^+}}}{\left(1 + \sqrt{\frac{L_{\{ABC\}}^+ R_{\{ABC\}}^-}{L_{\{ABC\}}^- R_{\{ABC\}}^+}}\right)^2} \tag{25}$$

Lastly, we also define ε_{ABC} , the asymmetry in the combined region A+B+C,

$$(\varepsilon_{ABC})_{LR} = \frac{1 - \sqrt{\frac{(\sum_{ABC} L^+) \cdot (\sum_{ABC} R^-)}{(\sum_{ABC} L^-) \cdot (\sum_{ABC} R^+)}}}{1 + \sqrt{\frac{(\sum_{ABC} L^+) \cdot (\sum_{ABC} R^-)}{(\sum_{ABC} L^-) \cdot (\sum_{ABC} R^+)}}} \tag{26}$$

with uncertainty derived using Equation 5.

With the definitions above we can discuss dilution from background events using the following quantities – in the plane that physics asymmetry exists in, we define dilution asymmetry DA as –

$$\langle DA \rangle [\%] = \left(1 - \frac{\varepsilon_{ABC}}{\varepsilon_B}\right) \cdot 100 \tag{27}$$

and then for each detector, dilution number $DN_{\{LRUD\}}$ – (replace $N_{\{ABC\}}$ with L, R, U or D)

$$\langle DN_{\{LRUD\}} \rangle [\%] = \frac{N_A + N_C}{2N_B} \cdot 100 \tag{28}$$

Dilution number $DN_{\{LRUD\}}$ provides an estimate of the percentage of events within our cuts that come

from background, per detector. It is only an estimate, however, and most useful when comparing between different foil thicknesses. The quantity only deals with the total number of events in each region, not the positive and negative helicity events independently. These events could carry analyzing power – be broken down by helicity in same ratios as that of “good” scatterings – and not dilute our final physics asymmetry. A better estimate of dilution from unpolarized background events is DA. The ratio $\epsilon_{ABC} / \epsilon_B$ is the crux. Dilution from unpolarized background events implies $\epsilon_{ABC} < \epsilon_B$ and so $\epsilon_{ABC} / \epsilon_B < 1$. The more diluting events, the less the ratio $\epsilon_{ABC} / \epsilon_B$ is, while fewer diluting events has $\epsilon_{ABC} / \epsilon_B$ approach unity. One minus this quantity (and scaled by 100), then, is a direct measure of the strength of dilution from background events we can expect.

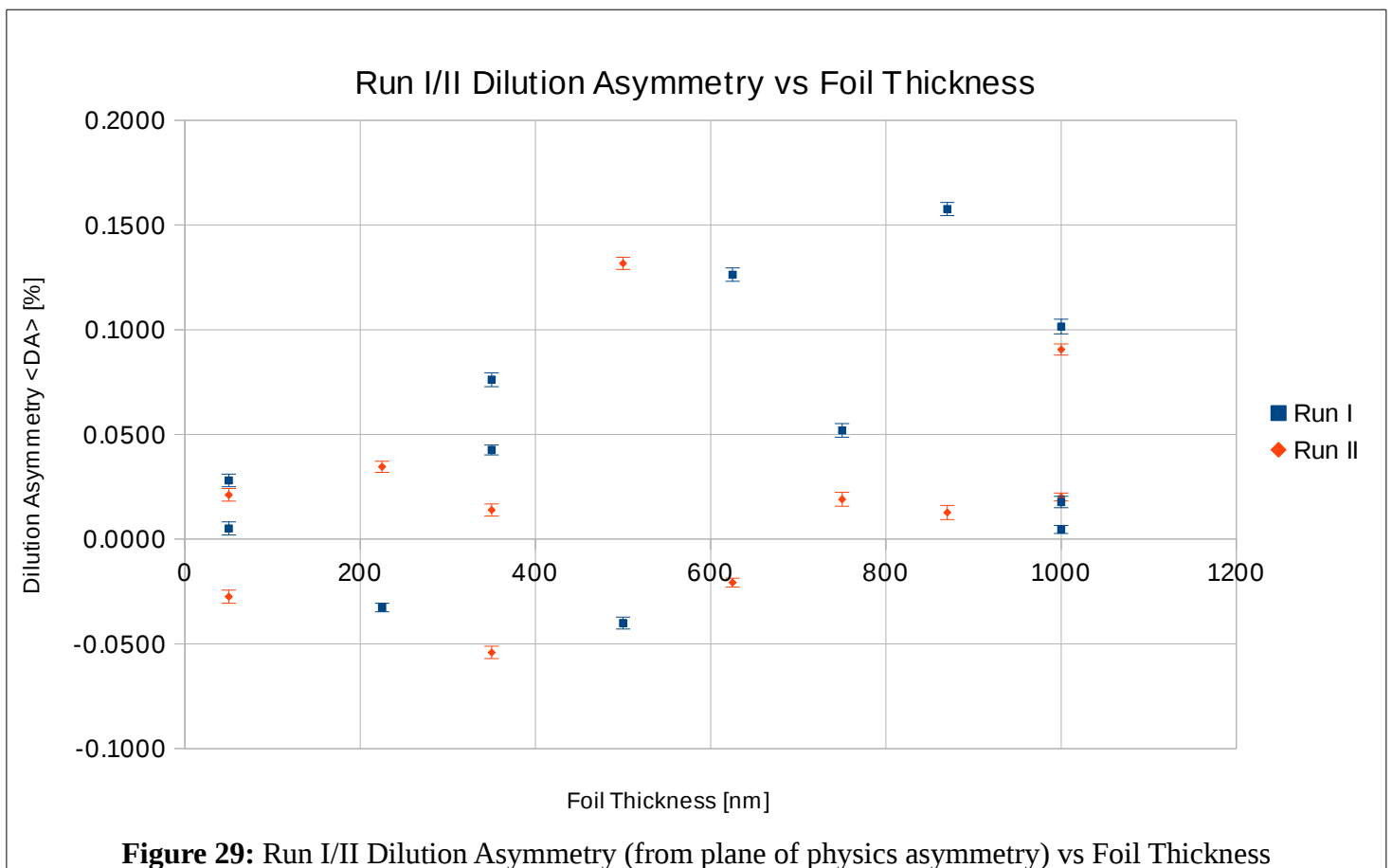
Run I, Up/Down Physics Asymmetry			Dilution Asymmetry <DA>		Dilution Number <DN>			
Threshold	Foil	Thickness [nm]	Asym [%]	dAsym [%]	LEFT [%]	RIGHT [%]	UP [%]	DOWN [%]
Low	15	1000	0.1015	0.0035	1.721	1.467	1.526	1.788
Low	3	870	0.1576	0.0031	1.752	1.441	1.452	1.650
Low	4	750	0.0520	0.0033	1.597	1.449	1.292	1.825
Low	2	625	0.1263	0.0032	1.539	1.363	1.274	1.525
Low	5	500	-0.0401	0.0028	1.485	1.451	1.217	1.806
Low	14	350	0.0761	0.0033	1.418	1.405	1.370	1.808
High	8	350	0.0426	0.0024	1.516	1.618	1.518	1.999
High	1	225	-0.0326	0.0020	1.444	1.581	1.341	1.848
High	12	50	0.0051	0.0031	1.445	1.659	1.439	1.840
High	13	50	0.0280	0.0030	1.488	1.616	1.452	1.876
Low	15 – stability	1000	0.0177	0.0027	1.636	1.534	1.538	1.853
High	15 – stability	1000	0.0046	0.0019	1.834	1.750	1.851	2.136

Table 13

Run II, Left/Right Physics Asymmetry		Dilution Asymmetry <DA>		Dilution Number <DN>			
Foil	Thickness [nm]	Asym [%]	dAsym [%]	LEFT [%]	RIGHT [%]	UP [%]	DOWN [%]
15	1000	0.0905	0.0026	1.708	1.795	1.762	1.773
3	870	0.0127	0.0033	1.684	1.603	1.634	1.416
4	750	0.0190	0.0033	1.728	1.741	1.507	1.790
2	625	-0.0207	0.0021	1.649	1.608	1.477	1.321
5	500	0.1317	0.0029	1.671	1.834	1.587	1.879
14	350	-0.0541	0.0030	1.692	1.681	1.705	1.676
8	350	0.0139	0.0029	1.736	1.714	1.821	1.606
1	225	0.0345	0.0026	1.572	1.619	1.454	1.384
12	50	0.0211	0.0030	1.199	1.400	1.529	1.361
13	50	-0.0274	0.0031	1.060	1.299	1.588	1.274
15 – stability	1000	0.0201	0.0018	1.667	1.805	1.791	1.789

Table 14

Tables 13 and 14 present results from Asymmetry versus Foil Thickness runs from Run I and Run II. DA for the plane physics asymmetry occurred in and DN for each detector were calculated for each run and then runs on the same foil thickness were averaged together. For nearly all foil thicknesses, in both Runs I and II, the strength of asymmetry dilution DA is less than 0.1%, and never more than 0.16%. In Run I, the average DA across all foil thicknesses is 0.05% and in Run II 0.02%. The average dilution number DN across all four detectors is 1.6% from both Run I and Run II respectively. So, in our Mott data, we on average have up to 1.6% of events within our cuts coming from background and not the beam, diluting our physics asymmetry by on average less than 0.1%. Since this dilution is less than our statistical uncertainty, we do not include a correction for it.



Final Asymmetry Calculation

The final physics/Mott asymmetry uncertainty, Equation 29, is simply the statistical uncertainty added in quadrature with the systematic uncertainty due to choice of cuts.

$$\sigma_A = A\sqrt{(dA^{stat})^2 + (dA_{cuts}^{sys})^2} \quad (29)$$

Final Rate Calculation

The analysis code reports a rate per detector along with a statistical uncertainty. This rate is reported in Hz, so that when an average rate across multiple runs on the same foil is calculated, the beam currents per run can be arithmetically averaged together before inclusion in the final rate calculation of units Hz/uA.

The polarimeter is designed to precisely measure asymmetry calculated using the cross ratio method, not rate. As such, while the asymmetry is unaffected by beam drift, rates will change. To account for this drift, the stability runs on the 1 micron foil, taken in between each set of runs on a given foil thickness, and asymmetry-data runs on the 1 micron foil, were examined. From the spread of the average rate in Hz of these runs a drift uncertainty was calculated as –

$$(\text{Max} - \text{Min}) / (\text{Max} + \text{Min}) = \text{Drift Uncertainty} = |\Delta/\Sigma| \quad (30)$$

Drift Uncertainty for Run I = 1.55%, and for Run II = 1.51% . This systematic uncertainty is added in quadrature with the other rate uncertainties.

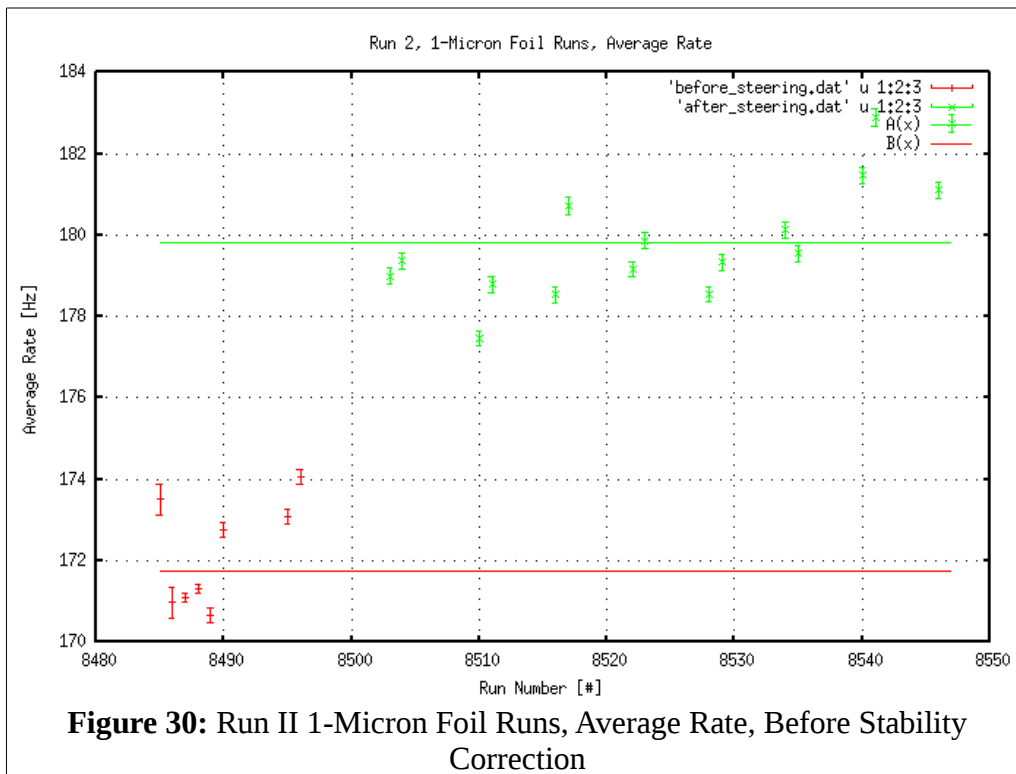
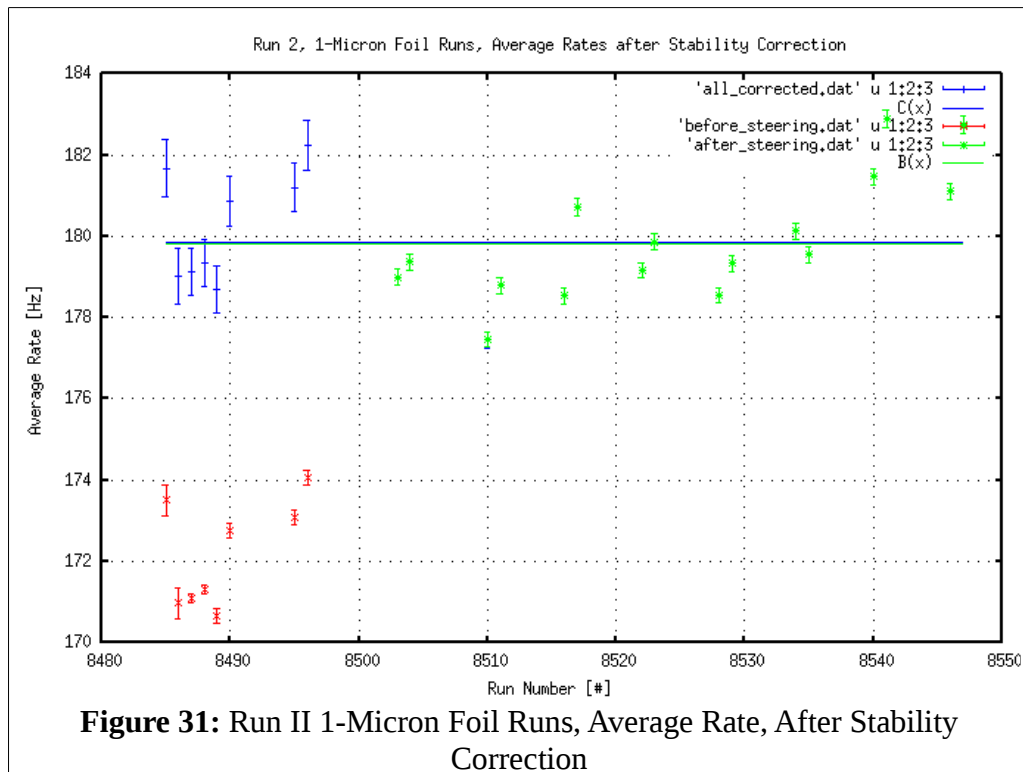


Figure 30: Run II 1-Micron Foil Runs, Average Rate, Before Stability Correction

When looking at the drift in average rate across 1-micron-foil-runs from Run II, it was noticed that the first eight runs reported a 10% smaller rate than all subsequent ones. No difference between these smaller-rate runs and the rest was seen in asymmetry. Run I did not exhibit such a large difference between average rate of any two runs on the 1 micron foil. The difference in setup in Run II between these runs was traced back to magnet beam steering. These smaller-rate runs were taken while the beam was not well-centered in our experimental beamline. This steering error was corrected in between data-taking runs. As such, for these eight 1 micron foil runs and all other runs on other foils taken during this period of beam scraping, a stability correction was calculated to be applied to the rates. This was done by calculating the average rate of runs on the 1 micron foil when beam was scraping (the red points in Figure 24, $B(x) = B =$ before steering), along with the average rate of runs on the 1 micron foil after correcting the scraping (the green points in Figure 30, $A(x) = A =$ after steering). Then, a stability correction C was calculated as –

$$\text{Stability Correction } C = \text{Average Rate After Steering } A / \text{Average Rate Before Steering } B \quad (31)$$

For these Run II runs, the stability correction $C = 1.0470 \pm 0.0033$. Figure 31 shows the uncorrected Run II rates in red and the corrected ones in blue. The green points are rates after the steering correction was made. The green line is the average of rates after steering correction, while the blue line



is the average of rates after stability correction applied. These lines are the same.

The correction is applied to the specified runs outside of the analysis code, directly to the rates in Hz that are reported by the code. Only after this correction is applied to the Run II rates is the Run II Drift Uncertainty calculated. No such stability correction was found necessary in the Run I Rate data.

From the analysis code's output, a run's final rate, either average or per detector, can be calculated as –

$$R^{final}[Hz/\mu A] = \frac{R^{code}[Hz]}{I[\mu A]} \cdot C \quad (32)$$

The code also reports a statistical uncertainty in rate, Equation 16, dR^{code} [Hz], that when accounting for stability correction, becomes –

$$dR^{stat}[Hz/\mu A] = \frac{\sqrt{C^2 \cdot (dR^{code})^2 + (R^{code})^2 \cdot dC^2}}{I} \quad (33)$$

Then, this can be combined with our systematic uncertainties to form a final rate uncertainty –

$$\sigma_R = R^{final}[Hz/\mu A] \sqrt{\left(\frac{dR^{stat}}{R^{final}}\right)^2 + \left(\frac{dI}{I}\right)^2 + \left|\frac{\Delta}{\Sigma}\right|^2 + (dR_{cuts}^{syst})^2} \quad (34)$$

Run I Results

Table 15 summarizes Run I Asymmetry versus Foil Thickness results. For a complete table of all asymmetries – both Left-Right and Up-Down plane physics, beam-instrumental, and detector-instrumental – see Appendix ##. Table 16 summarizes Average Rate results from the same runs. For a complete table of Rates broken down by detector and all systematic and statistical uncertainties, see Appendix ##.

Run I Physics Asymmetry Results						
PMT Threshold	Foil #	Nominal Thickness	FESEM Thickness	FESEM Thickness Uncertainty	Physics Asymmetry	Physics Asymmetry Uncertainty
high/low	#	T_0 [nm]	T [nm]	σ_T [nm]	A [%]	σ_A [%]
Low	15	1000	943.7	59.8	33.963	0.092
Low	3	870	836.8	44.2	34.846	0.089
Low	4	750	774.6	41.9	35.720	0.093
Low	2	625	561.2	31.0	37.352	0.096
Low	5	500	482.0	27.7	38.786	0.095
Low	14	350	389.4	22.1	39.255	0.103
High	8	350	389.4	22.1	39.233	0.096
High	1	225	215.2	11.7	40.973	0.084
High	12	50	50.0	5.0	43.298	0.103
High	13	50	52.0	4.7	43.533	0.101
Low	15 – stability	1000	943.7	59.8	33.780	0.070
High	15 – stability	1000	943.7	59.8	33.844	0.060

Table 15

Run I Average Rate Results						
PMT Threshold	Foil #	Nominal Thickness	FESEM Thickness	FESEM Thickness Uncertainty	Average Rate	Average Rate Uncertainty
high/low	#	T_0 [nm]	T [nm]	σ_T [nm]	R [Hz/uA]	σ_R [Hz/uA]
Low	15	1000	943.7	59.8	186.769	3.441
Low	3	870	836.8	44.2	159.211	3.051
Low	4	750	774.6	41.9	135.752	2.497
Low	2	625	561.2	31.0	97.702	1.738
Low	5	500	482.0	27.7	74.123	1.294
Low	14	350	389.4	22.1	61.497	1.045
High	8	350	389.4	22.1	61.530	1.007
High	1	225	215.2	11.7	34.650	0.565
High	12	50	50.0	5.0	7.240	0.118
High	13	50	52.0	4.7	7.420	0.121
Low	15	1000	943.7	59.8	188.245	3.450
High	15	1000	943.7	59.8	189.740	3.452

Table 16

Run II Results

Table 17 summarizes Run II Asymmetry versus Foil Thickness results. For a complete table of all asymmetries – both Left-Right and Up-Down plane physics, beam-instrumental, and detector-instrumental – see Appendix ##. Table 18 summarizes Average Rate results from the same runs. For a complete table of Rates broken down by detector and all systematic and statistical uncertainties, see Appendix ##.

Run II Physics Asymmetry Results					
Foil #	Nominal Thickness	FESEM Thickness	FESEM Thickness Uncertainty	Physics Asymmetry	Physics Asymmetry Uncertainty
#	T_0 [nm]	T [nm]	σ_T [nm]	A [%]	σ_A [%]
15	1000	943.7	59.8	33.972	0.083
3	870	836.8	44.2	34.954	0.102
4	750	774.6	41.9	35.910	0.104
2	625	561.2	31.0	37.167	0.087
5	500	482.0	27.7	38.771	0.105
14	350	389.4	22.1	39.156	0.108
8	350	389.4	22.1	39.360	0.107
1	225	215.2	11.7	40.933	0.106
12	50	50.0	5.0	43.446	0.120
13	50	52.0	4.7	43.432	0.119
15 – stability	1000	943.7	59.8	34.005	0.051

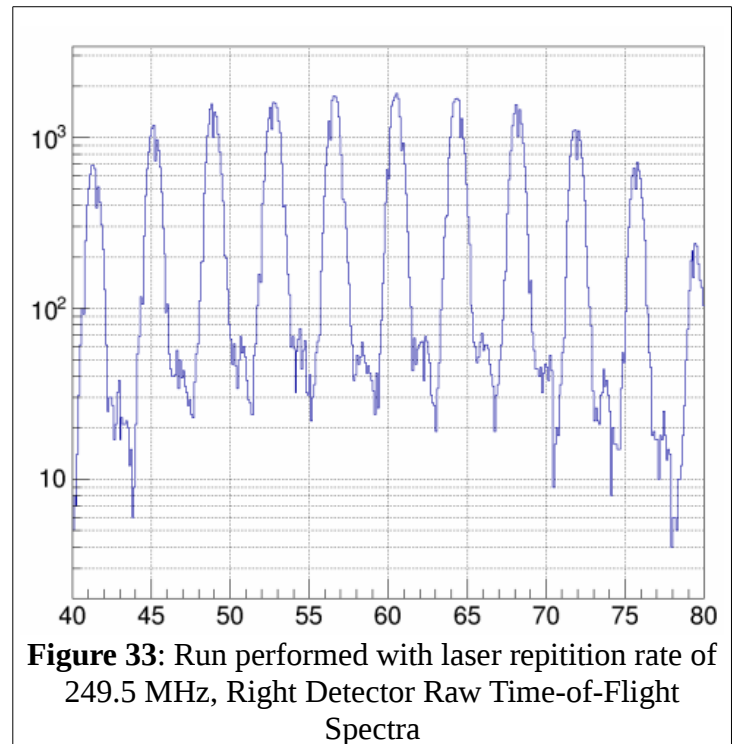
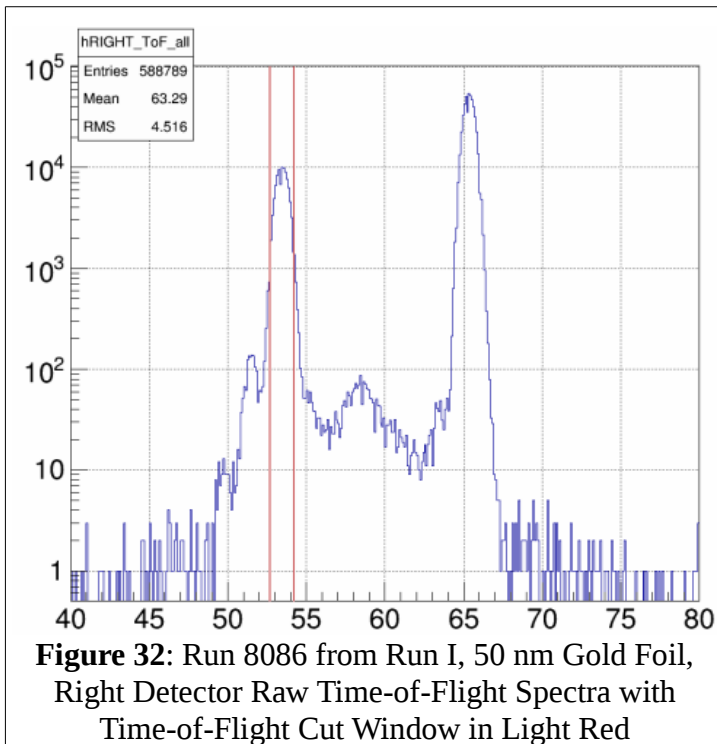
Table 17

Run I Average Rate Results					
Foil #	Nominal Thickness	FESEM Thickness	FESEM Thickness Uncertainty	Average Rate	Average Rate Uncertainty
#	T_0 [nm]	T [nm]	σ_T [nm]	R [Hz/uA]	σ_R [Hz/uA]
15	1000	943.7	59.8	179.708	3.169
3	870	836.8	44.2	152.667	2.695
4	750	774.6	41.9	129.469	2.284
2	625	561.2	31.0	94.607	1.670
5	500	482.0	27.7	70.454	1.246
14	350	389.4	22.1	58.046	1.027
8	350	389.4	22.1	60.092	1.061
1	225	215.2	11.7	33.813	0.597
12	50	50.0	5.0	7.057	0.112
13	50	52.0	4.7	7.084	0.113
15	1000	943.7	59.8	179.840	3.174

Table 18

Asymmetry Without Time-of-Flight Cut

During Mott data Runs I and II the laser used to illuminate the gun cathode and create electron beam was setup at 31MHz, giving 32 ns between electron beam bunches. This was done so that separate target scattering and dump scattering peaks could be resolved in the time-of-flight spectra. From Figure 29, Run I, run 8086 on 50 nm gold foil, Right Detector Time-of-Flight Spectra with no hardware timing veto, at ~ 53.5 ns we see a peak from target scatterings and at ~ 66 ns an even larger peak corresponding to dump scatterings. These peaks are ~ 12 ns apart, requiring sub-100MHz laser repetition frequency to resolve, a fraction of normal CEBAF operating laser repetition rates of 249.5 and 499 MHz. Figure 33 shows an example of a ToF spectra from a run where the laser repetition rate was



249.5 MHz – many peaks ~ 4 ns apart, but none directly corresponding to either target or dump scatterings and so no ToF cut can be employed. There is benefit, then, in understanding how our final results differ from when a ToF cut is employed versus when one is not.

To study the effect of not having a ToF cut, Run I and II Asymmetry versus Foil Thickness data was run through the analysis code both with and without a ToF cut, and then fit using our standard Asymmetry versus Foil Thickness Pade fit forms – the simulation-predicted Pade(1,1), equation 19; the next best Pade fit form, a Pade(0,1), equation 20; and a quadratic form, a Pade(2,0), equation 32. Results were then compared.

$$A(t) = \frac{a_0 + a_1 t}{1 + a_2 t} \quad (19 \text{ duplicate})$$

$$A(t) = \frac{a_0}{1 + a_1 t} \quad (20 \text{ duplicate})$$

$$A(t) = a_0 + a_1 t + a_2 t^2 \quad (35)$$

Table 19 presents Run I data, with the column Difference = ToF Cut Asymmetry – Not ToF Cut Asymmetry. Table 20 presents Run II data.

Run I ToF vs Not ToF Cut			ToF Cut		Not ToF Cut		Difference
Threshold	Foil	Thickness [nm]	A [%]	dA [%]	A [%]	dA [%]	A(ToF Cut) – A(Not ToF Cut) [%]
Low	15	1000	33.963	0.092	33.925	0.090	0.038
Low	3	870	34.846	0.089	34.786	0.088	0.060
Low	4	750	35.720	0.093	35.692	0.092	0.028
Low	2	625	37.352	0.096	37.293	0.095	0.059
Low	5	500	38.786	0.095	38.776	0.093	0.010
Low	14	350	39.255	0.103	39.212	0.101	0.043
High	8	350	39.233	0.096	39.199	0.095	0.034
High	1	225	40.973	0.084	40.971	0.083	0.003
High	12	50	43.298	0.103	43.257	0.101	0.042
High	13	50	43.533	0.101	43.482	0.099	0.051
Low	15 – stability	1000	33.780	0.070	33.766	0.069	0.014
High	15 – stability	1000	33.844	0.060	33.834	0.058	0.010

Table 19

Run II ToF vs Not ToF Cut		ToF Cut		Not ToF Cut		Difference
Foil	Thickness [nm]	A [%]	dA [%]	A [%]	dA [%]	A(ToF Cut) – A(Not ToF Cut) [%]
15	1000	33.972	0.083	33.946	0.082	0.026
3	870	34.954	0.102	34.945	0.100	0.009
4	750	35.910	0.104	35.891	0.102	0.019
2	625	37.167	0.087	37.172	0.085	-0.005
5	500	38.771	0.105	38.711	0.104	0.060
14	350	39.156	0.108	39.175	0.106	-0.019
8	350	39.360	0.107	39.357	0.105	0.003
1	225	40.933	0.106	40.913	0.104	0.020
12	50	43.446	0.120	43.423	0.119	0.024
13	50	43.432	0.119	43.426	0.117	0.007
15 – stability	1000	34.005	0.051	33.993	0.050	0.012

Table 20

On all foils in Run I, and all but two in Run II, the asymmetry decreases when a ToF cut is not employed versus when one is, but by less than a tenth of a percent. The change is always within the uncertainty of both ToF Cut and Not ToF Cut data sets.

Figure 34 shows ToF cut data in blue and not ToF cut data in red for Run I, and Figure 35 shows Run II. In each, the simulation-predicted Pade(1,1) fit form is displayed for each set of data in its respective color scheme. Figures for the other two fit forms are presented in Appendix ##.

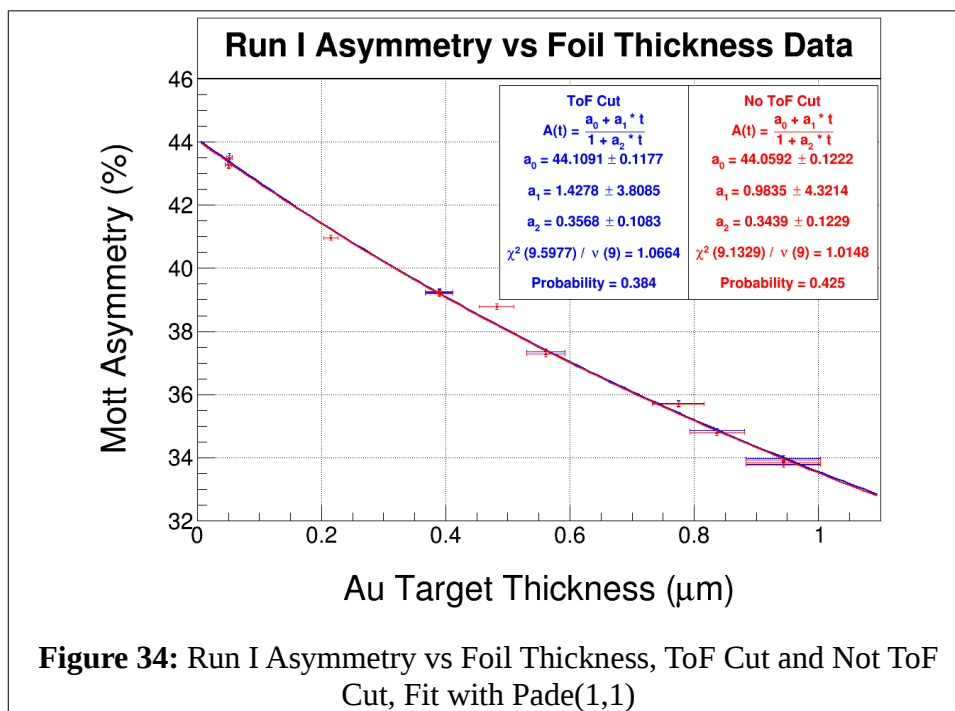


Figure 34: Run I Asymmetry vs Foil Thickness, ToF Cut and Not ToF Cut, Fit with Pade(1,1)

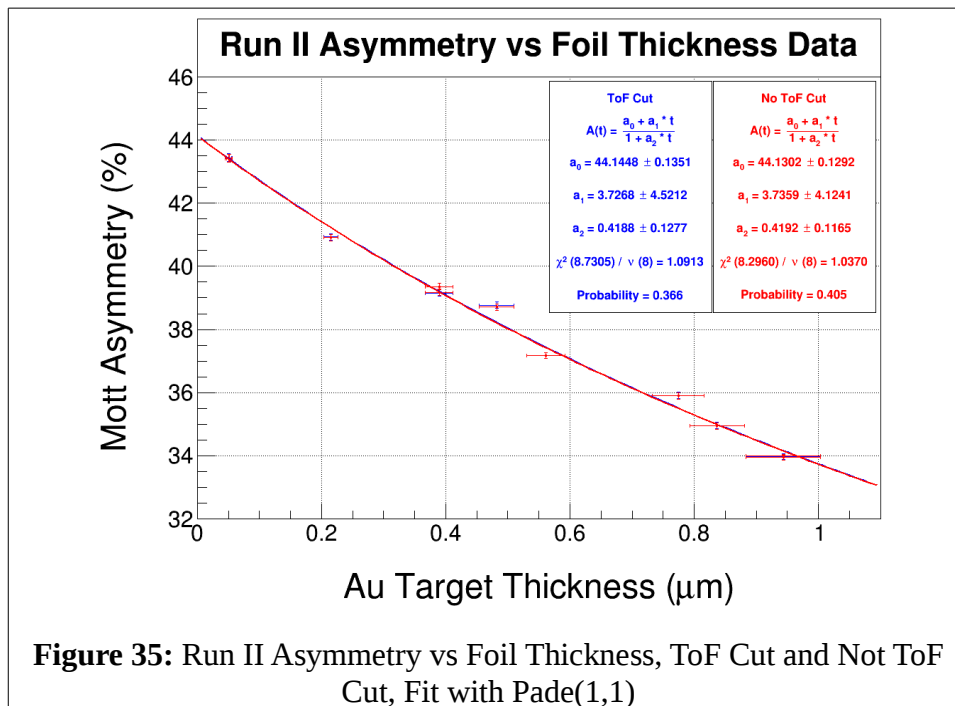


Figure 35: Run II Asymmetry vs Foil Thickness, ToF Cut and Not ToF Cut, Fit with Pade(1,1)

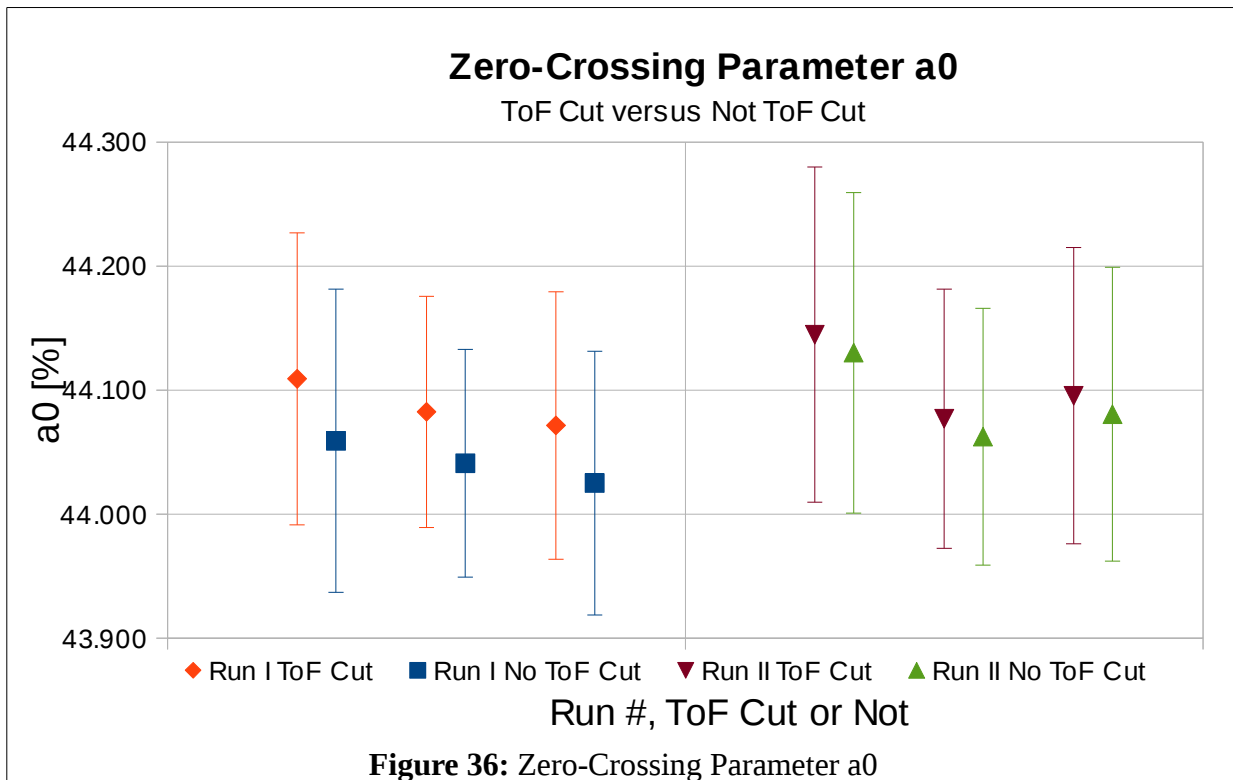
Tables 21 and 22 present fit parameter results for all three fits, for Run I and II respectively. Figure 36 shows zero-crossing parameter a_0 from the three fits considered, ToF and Not ToF Cut, Run I and II.

Run I Asymmetry versus Foil Thickness Fit Parameters, ToF Cut vs Not ToF Cut									
Fit	Cut?	a_0	$d(a_0)$	a_1	$d(a_1)$	a_2	$d(a_2)$	Chi ² / NDF	Probability
Pade(1,1)	ToF Cut	44.109	0.118	1.428	3.808	0.357	0.108	1.066	0.384
	No ToF Cut	44.059	0.122	0.984	4.321	0.344	0.123	1.015	0.425
	Difference	0.050		0.444		0.013			
Pade(0,1)	ToF Cut	44.083	0.093	0.316	0.008			0.974	0.464
	No ToF Cut	44.041	0.092	0.316	0.008			0.920	0.513
	Difference	0.041		0.000					
Pade(2,0)	ToF Cut	44.072	0.108	-13.641	0.763	3.134	0.836	1.150	0.323
	No ToF Cut	44.025	0.106	-13.553	0.763	3.051	0.841	1.085	0.370
	Difference	0.046		-0.088		0.082			

Table 21

Run II Asymmetry versus Foil Thickness Fit Parameters, ToF Cut vs Not ToF Cut									
Fit	Cut?	a_0	$d(a_0)$	a_1	$d(a_1)$	a_2	$d(a_2)$	Chi ² / NDF	Probability
Pade(1,1)	ToF Cut	44.145	0.135	3.727	4.521	0.419	0.128	1.091	0.366
	No ToF Cut	44.130	0.129	3.736	4.124	0.419	0.117	1.037	0.405
	Difference	0.015		-0.009		0.000			
Pade(0,1)	ToF Cut	44.077	0.104	0.314	0.009			1.051	0.396
	No ToF Cut	44.063	0.103	0.314	0.009			1.004	0.434
	Difference	0.014		0.000					
Pade(2,0)	ToF Cut	44.096	0.120	-13.892	0.796	3.548	0.879	1.195	0.297
	No ToF Cut	44.081	0.118	-13.886	0.792	3.544	0.875	1.145	0.329
	Difference	0.015		-0.006		0.004			

Table 22



From Figure 36 we see that our final fit parameter a_0 that describes the polarimeter's analyzing power is reduced slightly when ToF cuts are not used. The reduction, however, is within the uncertainty of when ToF cuts are used. If a no-ToF-cut correction were to be applied, it would at most be on the order of a tenth of a percent of the final value a_0 . (Run I Pade(1,1) case where difference in a_0 the greatest: $(0.05 / 44.13) * 100 = 0.11 \%$).